INTERNATIONAL JOURNAL FOR NUMERICAL METHODS IN ENGINEERING
Int. J. Numer. Meth. Engng 2010; **83**:1376–1406
Published online 4 May 2010 in Wiley InterScience (www.interscience.wiley.com). DOI: 10.1002/nme.2872

A family of ANS four-node exact geometry shell elements in general convected curvilinear coordinates

G. M. Kulikov*, † and S. V. Plotnikova

Department of Applied Mathematics and Mechanics, Tambov State Technical University, Sovetskaya Street, 106, Tambov 392000, Russia

SUMMARY

The non-conventional exact geometry shell elements based on the Timoshenko–Mindlin kinematics with five displacement degrees of freedom are proposed. The term 'exact geometry (EXG)' reflects the fact that coefficients of the first and second fundamental forms of the reference surface and Christoffel symbols are taken exactly at every Gauss integration point. The choice of only displacements as fundamental shell unknowns gives an opportunity to derive strain–displacement relationships, which are invariant under rigid-body shell motions in a convected curvilinear coordinate system. This paper presents a newly developed family consisting of three hybrid and one displacement-based four-node EXG shell elements. To avoid shear and membrane locking and have no spurious zero energy modes, the ANS concept is employed. The ANS interpolations satisfy exactly the plate compatibility equation for in-plane strains. As a result, all EXG shell elements developed pass membrane and bending plate patch tests and exhibit a superior performance in the case of distorted coarse mesh configurations. Copyright © 2010 John Wiley & Sons, Ltd.

Received 17 April 2008; Revised 29 May 2009; Accepted 18 January 2010

KEY WORDS: exact geometry shell element; 5-parameter shear deformation shell theory; assumed natural strain method; hybrid stress, hybrid strain and hybrid stress–strain methods

1. INTRODUCTION

A large number of works have been carried out on the degenerated shell elements [1] that can handle analyses of thin shells satisfactorily. These elements are typically defined by five displacement and rotation degrees of freedom per node and allow us to utilize distorted meshes efficiently. In the isoparametric degenerated shell element formulation, initial and deformed geometry are equally

*Correspondence to: G. M. Kulikov, Department of Applied Mathematics and Mechanics, Tambov State Technical University, Sovetskaya Street, 106, Tambov 392000, Russia.
†E-mail: kulikov@apmath.tstu.ru

Contract/grant sponsor: Russian Foundation for Basic Research; contract/grant number: 08-01-00373
Contract/grant sponsor: Russian Ministry of Education and Science; contract/grant number: 2.1.1/660

interpolated that permits one to describe rigid-body shell motions precisely. The development of degenerated shell elements is not straightforward [2–5]. In order to overcome element deficiencies such as shear and membrane locking, advanced finite element techniques including the assumed natural strain (ANS) method and hybrid stress and/or strain methods were employed. Still, the isoparametric degenerated shell element formulation is computationally inefficient because stresses and strains are analyzed in the global and local orthogonal Cartesian coordinate systems, although the normalized element coordinates represent already convected curvilinear coordinates.

An alternative way is to develop the exact geometry shell elements based on the extensive use of the general convected curvilinear coordinates. This finite element formulation also allows utilizing the distorted meshes and finds its point of departure in papers [6–12], devoted to the 5-parameter shear deformation shell theory [6, 8, 10] and the 6-, 7- and 9-parameter shell theories accounting for thickness stretching [7, 9, 11, 12]. The term 'exact geometry (EXG)' reflects the fact that coefficients of the first and second fundamental forms of the reference surface and Christoffel symbols are taken exactly at every Gauss integration point. The feature of above EXG shell elements is that they are based on the strain–displacement relationships, which precisely represent all rigid-body shell motions in a convected curvilinear coordinate system. This fact is of great importance since one may read in paper [13] that 'shell theory is an absolute academic exercise' due to 'the difficulties of representing the rigid body modes in shell finite element formulations'.

It should be noted that the EXG shell elements can handle the membrane-bending coupling properly but they cannot be readily implemented for the analysis of general shell structures, where no explicit description of the shell reference surface exists. This is due to the fact that the geometric objects such as coefficients of the second fundamental form or curvatures of the reference surface are not easily accessible in a computational context. It is apparent, in such general cases, e.g. the fender or the hood in a modern car body, the degenerated shell elements have to be utilized. However, there are some important shell problems, in which the EXG shell element formulation has advantages compared with the conventional degenerated shell element formulations since it allows one to reduce the computational cost of numerical integration in the evaluation of the stiffness matrix [9, 11]. This is the case of pneumatic tires, which are the most widely used shell structures of commercial importance today. The reference surface of a tire is generated by rotation of the arbitrarily curve given on a plane by the discrete number of prescribed points. Fortunately, the closed-form description of the tire reference surface is provided through authors' numerical algorithm of smoothing the data by cubic spline functions [14]. Therefore, large-scale tire computations may be carried out by using the EXG shell elements efficiently [15].

The EXG finite element formulation developed utilizes the Timoshenko–Mindlin kinematics with five *displacement* degrees of freedom [6] and is based on the simple and effective approximation of shells via *curved four-node* quadrilateral shell elements. To avoid shear and membrane locking and have no spurious zero energy modes, the ANS concept is employed here. This concept has been developed for the isoparametric plate/shell elements in [16–19] and provides an excellent performance in the case of distorted meshes. Currently, it is well established that the most widespread isoparametric four-node shell element based on the Timoshenko–Mindlin kinematics is sensitive to shear locking. This is because of incorrect shear modes, which infect the pure bending element behavior. Such a defect can be cured by evaluating correct transverse shear strains at sampling points and interpolating them in more suitable continuity. In regards to a EXG shell element formulation, it is not simple to apply the ANS concept even for low-order EXG shell elements because additionally membrane locking occurs. This is due to the fact that the exact representation of the reference surface yields the explicit variation of curvatures and

DOI: 10.1002/nme

Christoffel symbols throughout the element. To overcome both locking phenomena, the transverse shear strains and in-plane ones as well should be evaluated at sampling points and interpolated inside the element following the usual ANS technique [10]. Our numerical experiments showed that such ANS four-node EXG shell element performs well but does not pass membrane and bending plate patch tests [20]. However, both patch tests can be passed if ANS interpolations employed satisfy the plate compatibility equation for in-plane strains exactly. In fact, this means that the higher-order terms need to be included into the interpolation of in-plane strains throughout the quadrilateral shell element. The four-node EXG shell element based on this enhanced ANS technique has demonstrated a superior performance in all benchmark problems when we used *coarse* meshes with *extremely high* distortion. We mention also that the element stiffness matrix has six, and only six, zero eigenvalues as required for satisfaction of the general rigid-body motion representation.

To improve the computational efficiency of the ANS low-order shell elements, a *hybrid* method can be applied. This method is based on the robust finite element formulation pioneered by Pian [21]. In such a formulation the displacements on the element boundary are assumed to provide displacement compatibility between elements, whereas internal stresses are assumed so as to satisfy the differential equilibrium equations. The Pian's work was originally based on the principle of the stationary complementary energy. Later, an alternative *assumed stress* method was proposed by applying the Hellinger–Reissner variational principle that simplifies the evaluation of the element stiffness matrix [22].

However, herein we do not use this terminology referring to Gallagher's proposal (see paper [23]), where it is said that 'the hybrid method in structural mechanics is defined at the one which is formulated by multivariable variational functional, yet the resulting matrix equations consist of only the nodal values of displacements as unknown'. Independently, the hybrid strain [24, 25] and hybrid stress–strain [26] shell elements were developed. The former is based on the modified Hellinger–Reissner functional in which displacements and strains are utilized as fundamental shell unknowns, whereas the latter departs from the Hu–Washizu functional depending on displacements, stresses and strains.

In the present paper, all three hybrid ANS four-node EXG shell elements, namely, hybrid stress, hybrid strain and hybrid stress–strain elements are studied by using a unified technique. This allows one to assess their advantages and disadvantages and to compare them with a displacement-based ANS shell element. In this context, we notice that a hybrid stress–strain ANS element permits the analytical integration of some matrices that yield the simple analytical matrix inversion. That is unusual for the isoparametric hybrid shell element formulation. At the same time the hybrid stress and hybrid strain ANS shell elements exhibit an excellent performance in all benchmark problems considered but require expensive numerical matrix inversions.

2. KINEMATIC DESCRIPTION OF UNDEFORMED SHELL

Let us consider a shell of the thickness h. The shell can be defined as a 3D body of volume V bounded by two outer surfaces Ω^- and Ω^+, located at the distances d^- and d^+ measured with respect to the reference surface Ω such that $h=d^-+d^+$, and the edge boundary surface Σ. The reference surface is assumed to be sufficiently smooth and without any singularities. Let the reference surface be referred to the convected curvilinear coordinates θ^1 and θ^2, whereas the coordinate θ^3 is oriented along the unit vector $\boldsymbol{a}_3=\boldsymbol{a}^3$ normal to the reference surface.

DOI: 10.1002/nme

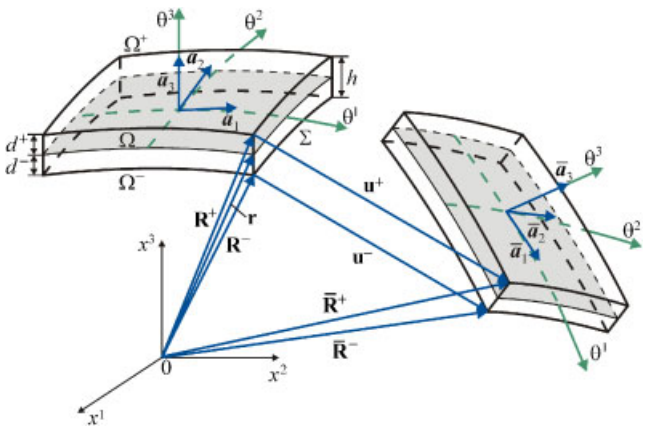

Figure 1. Initial and current configurations of the shell.

Introduce in accordance with Figure 1 the following notations: $\mathbf{r}=\mathbf{r}(\theta^1,\theta^2)$ is the position vector of any point of the reference surface; $\boldsymbol{a}_\alpha=\mathbf{r}_{,\alpha}$ are the covariant base vectors of the reference surface; $\boldsymbol{a}^\beta$ are the contravariant base vectors of the reference surface defined by the standard relation $\boldsymbol{a}_\alpha\cdot\boldsymbol{a}^\beta=\delta_\alpha^\beta$; $a_{\alpha\beta}=\boldsymbol{a}_\alpha\cdot\boldsymbol{a}_\beta$ and $a^{\alpha\beta}=\boldsymbol{a}^\alpha\cdot\boldsymbol{a}^\beta$ are the covariant and contravariant components of the metric tensor of the reference surface; $a=\det[a_{\alpha\beta}]$ is the determinant of the metric tensor of the reference surface; $b_\alpha^\beta=-\boldsymbol{a}^\beta\cdot\boldsymbol{a}_{3,\alpha}$ are the mixed components of the curvature tensor; $\mathbf{R}=\mathbf{r}+\theta^3\boldsymbol{a}_3$ is the position vector of any point in the shell body; in particular, $\mathbf{R}^I=\mathbf{r}+z^I\boldsymbol{a}_3$ are the position vectors of the bottom and top surfaces of the shell; $z^-=-d^-$ and $z^+=d^+$ are the transverse coordinates of the bottom and top surfaces; $\mu_\alpha^\beta=\delta_\alpha^\beta-\theta^3 b_\alpha^\beta$ are the mixed components of the 3D shifter tensor; in particular, $\mu_\alpha^{I\beta}=\delta_\alpha^\beta-z^I b_\alpha^\beta$ are the components of the shifter tensor at outer surfaces; $\mathbf{g}_i$ are the covariant base vectors in the shell body expressed as

$$\mathbf{g}_\alpha=\mathbf{R}_{,\alpha}=\mu_\alpha^\beta\boldsymbol{a}_\beta,\quad \mathbf{g}_3=\mathbf{R}_{,3}=\boldsymbol{a}_3 \tag{1}$$

in particular, base vectors of outer surfaces are

$$\mathbf{g}_\alpha^I=\mathbf{R}_{,\alpha}^I=\mu_\alpha^{I\beta}\boldsymbol{a}_\beta,\quad \mathbf{g}_3^I=\boldsymbol{a}_3, \tag{2}$$

g_{ij} are the covariant components of the 3D metric tensor given by

$$g_{\alpha\beta}=\mathbf{g}_\alpha\cdot\mathbf{g}_\beta=\mu_\alpha^\gamma\mu_\beta^\delta a_{\gamma\delta},\quad g_{i3}=\mathbf{g}_i\cdot\mathbf{g}_3=\delta_{i3}$$

in particular, components of the metric tensors of outer surfaces are

$$g_{\alpha\beta}^I=\mathbf{g}_\alpha^I\cdot\mathbf{g}_\beta^I=\mu_\alpha^{I\gamma}\mu_\beta^{I\delta}\boldsymbol{a}_{\gamma\delta},\quad g_{i3}^I=\mathbf{g}_i^I\cdot\mathbf{g}_3^I=\delta_{i3},$$

$g=\det[g_{ij}]$ is the determinant of the 3D metric tensor; $g^I=\det[g_{ij}^I]$ are the determinants of the metric tensors of outer surfaces; $\mu=\sqrt{g/a}$ is the determinant of the shifter tensor; $\mu^I=\sqrt{g^I/a}$ are the determinants of the shifter tensor at outer surfaces; $(\ldots)_{,i}$ are the partial derivatives in V with respect to coordinates θ^i; $(\ldots)|_\alpha$ are the covariant derivatives in Ω with respect to coordinates θ^α.

DOI: 10.1002/nme

Here and in the following developments, Greek tensorial indices range from 1 to 2; Latin tensorial indices i, j, m, n range from 1 to 3; indices I, J identify the belonging of any quantity to the bottom and top surfaces and take values $-$ and $+$.

3. KINEMATIC DESCRIPTION OF DEFORMED SHELL

Now, we introduce the first assumption for the proposed first-order shear deformation shell theory.

Assumption 1
The displacement field is approximated in the thickness direction according to the linear law (Timoshenko–Mindlin kinematics)

$$\mathbf{u}=\sum_I N^I\mathbf{u}^I, \tag{3}$$

$$\mathbf{u}^I=u^I_\alpha\boldsymbol{a}^\alpha+w\boldsymbol{a}^3, \tag{4}$$

where $u^I_\alpha(\theta^1,\theta^2)$ are the in-plane displacements of bottom and top surfaces; $w(\theta^1,\theta^2)$ is the transverse displacement; $N^I(\theta^3)$ are the polynomials of the first order defined as

$$N^-=\frac{1}{h}(z^+-\theta^3),\quad N^+=\frac{1}{h}(\theta^3-z^-), \tag{5}$$

such that $N^I(z^J)=1$ for $J=I$ and $N^I(z^J)=0$ for $J\neq I$.

The position vector of the deformed shell can be written as

$$\bar{\mathbf{R}}=\mathbf{R}+\mathbf{u}=\sum_I N^I\bar{\mathbf{R}}^I, \tag{6}$$

where $\bar{\mathbf{R}}^I(\theta^1,\theta^2)$ are the position vectors of outer surfaces expressed as

$$\bar{\mathbf{R}}^I=\mathbf{R}^I+\mathbf{u}^I. \tag{7}$$

The covariant base vectors in the current shell configuration are

$$\bar{\mathbf{g}}_\alpha=\bar{\mathbf{R}}_{,\alpha}=\sum_I N^I\bar{\mathbf{g}}^I_\alpha,\quad \bar{\mathbf{g}}_3=\bar{\mathbf{R}}_{,3}=\boldsymbol{a}_3+\boldsymbol{\beta}, \tag{8}$$

where $\bar{\mathbf{g}}^I_\alpha$ are the base vectors of outer surfaces of the deformed shell and $\boldsymbol{\beta}$ is the derivative of the displacement vector with respect to the transverse coordinate given by

$$\bar{\mathbf{g}}^I_\alpha=\bar{\mathbf{R}}^I_{,\alpha}=\mathbf{g}^I_\alpha+\mathbf{u}^I_{,\alpha}, \tag{9}$$

$$\boldsymbol{\beta}=\mathbf{u}_{,3}=\frac{1}{h}(\mathbf{u}^+-\mathbf{u}^-). \tag{10}$$

Taking into account the displacement presentation (4), we have

$$\boldsymbol{\beta}=\beta_\alpha\boldsymbol{a}^\alpha,\quad \beta_\alpha=\frac{1}{h}(u^+_\alpha-u^-_\alpha). \tag{11}$$

DOI: 10.1002/nme

4. STRAIN–DISPLACEMENT RELATIONSHIPS

The strain tensor can be written as

$$2\varepsilon_{ij}=\bar{\mathbf{g}}_i\cdot\bar{\mathbf{g}}_j-\mathbf{g}_i\cdot\mathbf{g}_j. \tag{12}$$

Substituting base vectors in initial and current shell configurations into relationships (12) and allowing for (9) and (11), one obtains the following expressions for the linearized strains of the 5-parameter shell theory:

$$\begin{aligned} 2\varepsilon_{\alpha\beta}&=\sum_{I,J}N^I N^J(\mathbf{u}^I_{,\alpha}\cdot\mathbf{g}^J_\beta+\mathbf{u}^J_{,\beta}\cdot\mathbf{g}^I_\alpha),\\ 2\varepsilon_{\alpha 3}&=\sum_{I}N^I(\mathbf{u}^I_{,\alpha}\cdot\boldsymbol{a}_3+\boldsymbol{\beta}\cdot\mathbf{g}^I_\alpha),\quad \varepsilon_{33}=0. \end{aligned} \tag{13}$$

It is seen from (5) and (13) that in-plane strains are the polynomials of the second order, whereas transverse shear strains are the polynomials of the first order through the shell thickness. To simplify the proposed shear deformation shell theory, we introduce the next assumption.

Assumption 2
From the computational point of view it is important to accept the simplest strain distribution, that is,

$$\begin{aligned} \widehat{\varepsilon}_{\alpha\beta}&=\sum_I N^I\varepsilon^I_{\alpha\beta},\\ \widehat{\varepsilon}_{\alpha 3}&=\varepsilon^{\mathrm{M}}_{\alpha 3},\quad \varepsilon^{\mathrm{M}}_{\alpha 3}=\tfrac{1}{2}(\varepsilon^-_{\alpha 3}+\varepsilon^+_{\alpha 3}),\quad \widehat{\varepsilon}_{33}=0. \end{aligned} \tag{14}$$

Here, $\varepsilon^I_{\alpha\beta}=\varepsilon_{\alpha\beta}(z^I)$ and $\varepsilon^I_{\alpha 3}=\varepsilon_{\alpha 3}(z^I)$ are the *exact values* of in-plane and transverse shear strains at the bottom and top surfaces, $\varepsilon^{\mathrm{M}}_{\alpha 3}$ are the transverse shear strains of the midsurface defined as

$$\begin{aligned} 2\varepsilon^I_{\alpha\beta}&=\mathbf{u}^I_{,\alpha}\cdot\mathbf{g}^I_\beta+\mathbf{u}^I_{,\beta}\cdot\mathbf{g}^I_\alpha,\\ 2\varepsilon^I_{\alpha 3}&=\mathbf{u}^I_{,\alpha}\cdot\boldsymbol{a}_3+\boldsymbol{\beta}\cdot\mathbf{g}^I_\alpha,\quad 2\varepsilon^{\mathrm{M}}_{\alpha 3}=\mathbf{u}^{\mathrm{M}}_{,\alpha}\cdot\boldsymbol{a}_3+\boldsymbol{\beta}\cdot\mathbf{g}^{\mathrm{M}}_\alpha, \end{aligned} \tag{15}$$

where $\mathbf{u}^{\mathrm{M}}$ and $\mathbf{g}^{\mathrm{M}}_\alpha$ are the displacement vector and base vectors of the midsurface:

$$\mathbf{u}^{\mathrm{M}}=\tfrac{1}{2}(\mathbf{u}^-+\mathbf{u}^+)=u^{\mathrm{M}}_\alpha\boldsymbol{a}^\alpha+w\boldsymbol{a}^3, \tag{16}$$

$$\mathbf{g}^{\mathrm{M}}_\alpha=\tfrac{1}{2}(\mathbf{g}^-_\alpha+\mathbf{g}^+_\alpha)=\mu^{\mathrm{M}\beta}_\alpha\boldsymbol{a}_\beta. \tag{17}$$

Remark 1
It can be verified by using (5) and (14) that in-plane components of the simplified and exact strain tensors satisfy the following linking condition:

$$\widehat{\varepsilon}_{\alpha\beta}(z^I)=\varepsilon_{\alpha\beta}(z^I)=\varepsilon^I_{\alpha\beta}.$$

This fact is illustrated in Figure 2.

DOI: 10.1002/nme

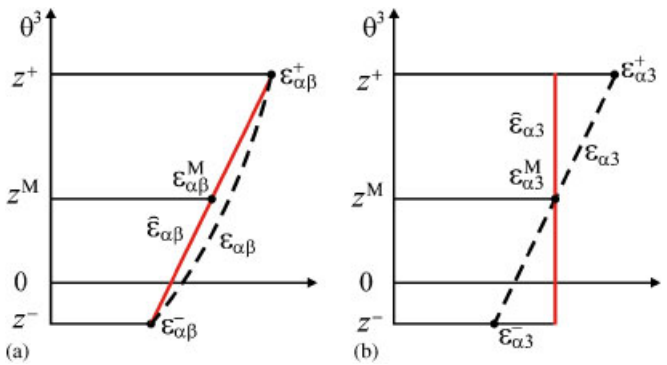

Figure 2. Approximate (——) and exact (− −) distributions of: (a) in-plane and (b) transverse shear strains through the thickness of the shell.

The derivatives of displacement vectors of outer and middle surfaces are written as

$$\begin{aligned} &\mathbf{u}^I_{,\alpha}=u^I_i|_\alpha \boldsymbol{a}^i, \quad \mathbf{u}^{\mathrm{M}}_{,\alpha}=u^{\mathrm{M}}_i|_\alpha \boldsymbol{a}^i, \\ &u^I_i|_\alpha=u^I_{i,\alpha}-\Gamma^j_{i\alpha}u^I_j, \quad u^{\mathrm{M}}_i|_\alpha=u^{\mathrm{M}}_{i,\alpha}-\Gamma^j_{i\alpha}u^{\mathrm{M}}_j, \end{aligned} \tag{18}$$

where for convenience it have been introduced the additional notations $u^I_3=u^{\mathrm{M}}_3=w$ and $\Gamma^j_{i\alpha}$ are the Christoffel symbols defined as

$$\Gamma^i_{\alpha\beta}=\boldsymbol{a}^i\cdot\boldsymbol{a}_{\alpha,\beta}, \quad \Gamma^\beta_{3\alpha}=-b^\beta_\alpha, \quad \Gamma^3_{3\alpha}=0. \tag{19}$$

Substituting (2), (11), (17) and (18) into strain–displacement relationships (15), we arrive at the index notations of these relationships

$$2\varepsilon^I_{\alpha\beta}=\mu^{I\gamma}_\beta u^I_\gamma|_\alpha+\mu^{I\gamma}_\alpha u^I_\gamma|_\beta, \quad 2\varepsilon^{\mathrm{M}}_{\alpha3}=u^{\mathrm{M}}_3|_\alpha+\mu^{\mathrm{M}\gamma}_\alpha\beta_\gamma. \tag{20}$$

Remark 2
The strains (14) are objective, i.e. they represent precisely rigid-body shell motions in any convected curvilinear coordinate system. A proof of this statement can be derived following a technique developed in [6, 7].

5. ANS FOUR-NODE EXG SHELL ELEMENTS

5.1. Principle of virtual work for 5-parameter shell element

The internal virtual work for the 3D shell element is expressed as

$$\delta W^{\mathrm{int}}_{\mathrm{el}}=\int\!\!\int_{\bar\Omega_{\mathrm{el}}}\int_{z^-}^{z^+}\mu\sigma^{ij}\delta\widehat{\varepsilon}_{ij}\sqrt{a}\,\mathrm{d}\theta^1\,\mathrm{d}\theta^2\,\mathrm{d}\theta^3, \tag{21}$$

where σ^{ij} are the contravariant components of the stress tensor.

DOI: 10.1002/nme

Substituting strains (14) into (21) and introducing stress resultants

$$H_I^{\alpha\beta}=\int_{z^-}^{z^+}\mu\sigma^{\alpha\beta}N^I\,\mathrm{d}\theta^3,\quad H^{\alpha 3}=\int_{z^-}^{z^+}\mu\sigma^{\alpha 3}\,\mathrm{d}\theta^3, \tag{22}$$

one finds

$$\delta W_{\mathrm{el}}^{\mathrm{int}}=\int\int_{\bar{\Omega}_{\mathrm{el}}}\left(\sum_I H_I^{\alpha\beta}\delta\varepsilon_{\alpha\beta}^I+H^{\alpha 3}\delta\varepsilon_{\alpha 3}^{\mathrm{M}}\right)\sqrt{a}\,\mathrm{d}\theta^1\,\mathrm{d}\theta^2. \tag{23}$$

This study focuses on the linear elastic materials. The natural choice for constitutive equations is the generalized Hooke's law, that is,

$$\sigma^{\alpha\beta}=C^{\alpha\beta\gamma\delta}\,\widehat{\varepsilon}_{\gamma\delta},\quad \sigma^{\alpha 3}=C^{\alpha 3\beta 3}\,\widehat{\varepsilon}_{\beta 3}, \tag{24}$$

where C^{ijmn} are the contravariant components of the material tensor.

The use of (14) and (24) in stress resultants (22) yields

$$H_I^{\alpha\beta}=\sum_J D_{IJ}^{\alpha\beta\gamma\delta}\varepsilon_{\gamma\delta}^J,\quad H^{\alpha 3}=D^{\alpha 3\beta 3}\varepsilon_{\beta 3}^{\mathrm{M}}, \tag{25}$$

where

$$D_{IJ}^{\alpha\beta\gamma\delta}=\int_{z^-}^{z^+}\mu C^{\alpha\beta\gamma\delta}N^IN^J\,\mathrm{d}\theta^3,\quad D^{\alpha 3\beta 3}=\int_{z^-}^{z^+}\mu C^{\alpha 3\beta 3}\,\mathrm{d}\theta^3. \tag{26}$$

Remark 3

To carry out the exact analytical integration in (26), the determinant of the 3D shifter tensor can be approximated through the shell thickness using the linear law

$$\mu=\sum_I N^I\mu^I,$$

where μ^I are the determinants of the shifter tensor at outer surfaces. For a thin shell one can assume that metrics of all surfaces parallel to the reference surface are identical and equal to the metric of the midsurface [6, 7]. This implies that in the case of choosing the midsurface as a reference surface the simplest approximation $\mu=1$ can be used.

Remark 4

The components C^{ijmn} of the material tensor in the covariant basis of the reference surface $\boldsymbol{a}_\alpha$, $\boldsymbol{a}_3$ can be represented through the components $\hat{C}^{ijmn}$ of this tensor in the orthonormal basis $\mathbf{e}_\alpha$, $\boldsymbol{a}_3$, whose directions coincide with the principal material directions, as follows:

$$\begin{aligned}
&C^{\alpha\beta\gamma\delta}=\hat{C}^{\kappa\lambda\mu\nu}m_\kappa^\alpha m_\lambda^\beta m_\mu^\gamma m_\nu^\delta,\quad C^{\alpha 3\beta 3}=\hat{C}^{\kappa 3\lambda 3}m_\kappa^\alpha m_\lambda^\beta,\\
&\hat{C}^{1111}=\frac{1}{\square}E_1,\quad \hat{C}^{2222}=\frac{1}{\square}E_2,\quad \hat{C}^{1122}=\frac{1}{\square}\nu_{12}E_2,\quad \hat{C}^{2211}=\frac{1}{\square}\nu_{21}E_1,\\
&\hat{C}^{1212}=G_{12},\quad \hat{C}^{1313}=G_{13},\quad \hat{C}^{2323}=G_{23},\quad \square=1-\nu_{12}\nu_{21},
\end{aligned} \tag{27}$$

where E_1, E_2, G_{12}, G_{13}, G_{23}, ν_{12} and ν_{21} are the engineering material constants and $m_\alpha^\beta=\mathbf{e}_\alpha\cdot\boldsymbol{a}^\beta$.

DOI: 10.1002/nme

Consider next the virtual work of the external loads

$$\delta W_{\mathrm{el}}^{\mathrm{ext}} = \int\!\!\int_{\bar{\Omega}_{\mathrm{el}}} (\mu^+ p_+^i \delta u_i^+ - \mu^- p_-^i \delta u_i^-)\sqrt{a}\,\mathrm{d}\theta^1\,\mathrm{d}\theta^2 + \delta \breve{W}_{\mathrm{el}}^{\mathrm{ext}}, \tag{28}$$

where $\delta \breve{W}_{\mathrm{el}}^{\mathrm{ext}}$ is the virtual work done by external loads acting on the boundary surface $\Sigma_{e\ell}$; p_-^i and p_+^i are the contravariant components of the traction vectors applied to the bottom and top surfaces.

The principle of the virtual work is now stated in a matrix form as

$$\int\!\!\int_{\bar{\Omega}_{\mathrm{el}}} (\delta\boldsymbol{\varepsilon}^{\mathrm{T}}\mathbf{D}\boldsymbol{\varepsilon} - \delta\mathbf{v}^{\mathrm{T}}\mathbf{p})\sqrt{a}\,\mathrm{d}\theta^1\,\mathrm{d}\theta^2 - \delta \breve{W}_{\mathrm{el}}^{\mathrm{ext}} = 0, \tag{29}$$

where $\mathbf{v}$ is the displacement vector[‡]; $\boldsymbol{\varepsilon}$ is the strain vector; $\mathbf{p}$ is the surface traction vector; $\mathbf{D}$ is the material constitutive stiffness matrix given by

$$\mathbf{v} = [u_1^-\ \ u_2^-\ \ w\ \ u_1^+\ \ u_2^+]^{\mathrm{T}}, \quad \boldsymbol{\varepsilon} = [\varepsilon_{11}^-\ \ \varepsilon_{11}^+\ \ \varepsilon_{22}^-\ \ \varepsilon_{22}^+\ \ 2\varepsilon_{12}^-\ \ 2\varepsilon_{12}^+\ \ 2\varepsilon_{13}^{\mathrm{M}}\ \ 2\varepsilon_{23}^{\mathrm{M}}]^{\mathrm{T}},$$

$$\mathbf{p} = [-\mu^- p_-^1\ \ -\mu^- p_-^2\ \ (-\mu^- p_-^3 + \mu^+ p_+^3)\ \ \mu^+ p_+^1\ \ \mu^+ p_+^2]^{\mathrm{T}},$$

$$\mathbf{D} = \begin{bmatrix} D_{--}^{1111} & D_{-+}^{1111} & D_{--}^{1122} & D_{-+}^{1122} & D_{--}^{1112} & D_{-+}^{1112} & 0 & 0 \\ & D_{++}^{1111} & D_{-+}^{1122} & D_{++}^{1122} & D_{-+}^{1112} & D_{++}^{1112} & 0 & 0 \\ & & D_{--}^{2222} & D_{-+}^{2222} & D_{--}^{2212} & D_{-+}^{2212} & 0 & 0 \\ & & & D_{++}^{2222} & D_{-+}^{2212} & D_{++}^{2212} & 0 & 0 \\ & & & & D_{--}^{1212} & D_{-+}^{1212} & 0 & 0 \\ & & & & & D_{++}^{1212} & 0 & 0 \\ & & & & & & D^{1313} & D^{1323} \\ \text{sym.} & & & & & & & D^{2323} \end{bmatrix}. \tag{30}$$

5.2. *Finite element discretization*

For the curved four-node shell element, the displacement field is approximated according to the standard C^0 interpolation

$$\mathbf{v} = \sum_r N_r \mathbf{v}_r, \tag{31}$$

where $\mathbf{v}_r = [u_{1r}^- u_{2r}^- w_r u_{1r}^+ u_{2r}^+]^{\mathrm{T}}$ are the displacement vectors of the element nodes; $N_r(\xi^1, \xi^2)$ are the bilinear shape functions of the element [5]; the index r denotes the number of nodes and ranges from 1 to 4. The surface traction vector is also assumed to vary bilinearly inside the element.

[‡]From this point, any vector of order M stands for the column matrix of order $M \times 1$.

DOI: 10.1002/nme

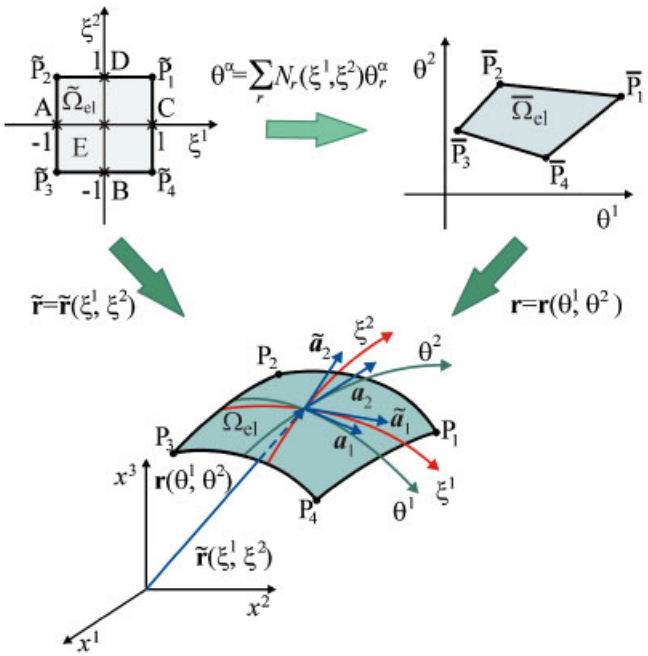

Figure 3. Biunit square in (ξ^1, ξ^2)-space mapped into the four-node exact geometry shell element in (x^1, x^2, x^3)-space.

Invoking bilinear shape functions [5], we can map a biunit square $\tilde{\Omega}_{el}=[-1, 1]\times[-1, 1]$ in (ξ^1, ξ^2)-space into any quadrilateral $\bar{\Omega}_{el}$ in (θ^1, θ^2)-space (Figure 3) by

$$\theta^\alpha=\sum_r N_r\theta_r^\alpha. \tag{32}$$

Therefore, a problem of finding the determinant of the transformation matrix

$$\begin{aligned}
&\Lambda=\det[t_\beta^\alpha],\\
&t_1^\alpha=\frac{\partial\theta^\alpha}{\partial\xi^1}=\frac{1}{4}(1+\xi^2)(\theta_1^\alpha-\theta_2^\alpha)+\frac{1}{4}(1-\xi^2)(\theta_4^\alpha-\theta_3^\alpha),\\
&t_2^\alpha=\frac{\partial\theta^\alpha}{\partial\xi^2}=\frac{1}{4}(1+\xi^1)(\theta_1^\alpha-\theta_4^\alpha)+\frac{1}{4}(1-\xi^1)(\theta_2^\alpha-\theta_3^\alpha)
\end{aligned} \tag{33}$$

arises. This determinant may be evaluated by means of a simple formula

$$\begin{aligned}
&\Lambda=c_0+c_\alpha\xi^\alpha,\\
&c_0=\tfrac{1}{8}[(\theta_1^1-\theta_3^1)(\theta_2^2-\theta_4^2)-(\theta_2^1-\theta_4^1)(\theta_1^2-\theta_3^2)],\\
&c_1=\tfrac{1}{8}[(\theta_1^1-\theta_2^1)(\theta_3^2-\theta_4^2)-(\theta_3^1-\theta_4^1)(\theta_1^2-\theta_2^2)],\\
&c_2=\tfrac{1}{8}[(\theta_1^1-\theta_4^1)(\theta_2^2-\theta_3^2)-(\theta_2^1-\theta_3^1)(\theta_1^2-\theta_4^2)].
\end{aligned} \tag{34}$$

DOI: 10.1002/nme

Further, it is convenient to introduce a displacement vector of the shell element

$$\mathbf{U}=[\mathbf{v}_1^{\mathrm{T}}\ \mathbf{v}_2^{\mathrm{T}}\ \mathbf{v}_3^{\mathrm{T}}\ \mathbf{v}_4^{\mathrm{T}}]^{\mathrm{T}}. \tag{35}$$

Substituting the interpolation (31) into strain–displacement relationships (20) and taking into account notations (30) and (35), one derives the following matrix equation:

$$\boldsymbol{\varepsilon}=\mathbf{B}\mathbf{U}, \tag{36}$$

where $\mathbf{B}(\xi^1, \xi^2)$ is the elemental strain–displacement transformation matrix of order 8×20.

5.3. ANS concept and four-node EXG shell elements

The pure displacement-based finite element formulation only makes sense when higher-order elements are employed. This is due to incorrect shear modes, which infect the pure bending plate/shell element behavior. Such a defect, known in the literature as shear locking, can be cured by evaluating correct transverse shear strains at sampling points and interpolating them inside the element in more suitable continuity.

5.3.1. Conventional ANS method for transverse shear strains. To overcome shear locking, a conventional ANS method for the transverse shear strains with four sampling points may be used (see e.g. [27], p. 274) and written in accordance with our notations as follows:

$$\begin{aligned}\tilde{\varepsilon}_{13}^M&=\tfrac{1}{2}(1-\xi^2)\,\tilde{\varepsilon}_{13}^M(B)+\tfrac{1}{2}(1+\xi^2)\,\tilde{\varepsilon}_{13}^M(D),\\ \tilde{\varepsilon}_{23}^M&=\tfrac{1}{2}(1-\xi^1)\,\tilde{\varepsilon}_{23}^M(A)+\tfrac{1}{2}(1+\xi^1)\tilde{\varepsilon}_{23}^M(C).\end{aligned} \tag{37}$$

Here, $\tilde{\varepsilon}_{\alpha 3}^M$ are the transverse shear components of the strain tensor in the contravariant basis $\tilde{\boldsymbol{a}}^\alpha$, $\tilde{\boldsymbol{a}}^3$ of the natural coordinate system given by a standard relation $\tilde{\boldsymbol{a}}_\alpha\cdot\tilde{\boldsymbol{a}}^\beta=\delta_\alpha^\beta$, where

$$\tilde{\boldsymbol{a}}_\alpha=\frac{\partial\tilde{\mathbf{r}}}{\delta\xi^\alpha}=t_\alpha^\beta\boldsymbol{a}_\beta,\quad \tilde{\boldsymbol{a}}^\beta=\ell_\alpha^\beta\boldsymbol{a}^\alpha, \tag{38}$$

where $\tilde{\mathbf{r}}(\xi^1, \xi^2)=\mathbf{r}(\theta^1, \theta^2)$ is the position vector of any point of the elemental reference surface Ω_{el} (Figure 3); $\tilde{\boldsymbol{a}}^3(\xi^1, \xi^2)=\boldsymbol{a}^3(\theta^1, \theta^2)$ is the unit vector normal to the surface Ω_{el}; $\ell_\alpha^\beta=\partial\xi^\beta/\partial\theta^\alpha$ are the elements of the inverse Jacobian matrix expressed as

$$\ell_1^1=\frac{1}{\Lambda}t_2^2,\quad \ell_1^2=-\frac{1}{\Lambda}t_1^2,\qquad \ell_2^1=-\frac{1}{\Lambda}t_2^1,\quad \ell_2^2=\frac{1}{\Lambda}t_1^1. \tag{39}$$

The values of the transverse shear strains at sampling points A, B, C and D, located at the center of each edge of the biunit square, can be calculated using equations

$$2\tilde{\varepsilon}_{\alpha 3}^M=\frac{\partial w}{\partial\xi^\alpha}-\frac{1}{h}\tilde{\mu}_\alpha^{+\beta}\tilde{u}_\beta^-+\frac{1}{h}\tilde{\mu}_\alpha^{-\beta}\tilde{u}_\beta^+, \tag{40}$$

$$\tilde{u}_\beta^I=t_\beta^\gamma u_\gamma^I,\quad \tilde{\mu}_\alpha^{I\beta}=\delta_\alpha^\beta-z^I\tilde{b}_\alpha^\beta,\quad \tilde{b}_\alpha^\beta=t_\alpha^\gamma\ell_\delta^\beta b_\gamma^\delta, \tag{41}$$

which follow from strain–displacement relationships (20) and standard tensor transformations.

DOI: 10.1002/nme

Using interpolation (31) into the strain–displacement equations for in-plane components (20) and transverse shear ones (37) and (40) in conjunction with (41) and

$$\varepsilon^M_{\alpha 3} = \ell^\beta_\alpha \tilde{\varepsilon}^M_{\beta 3}, \tag{42}$$

recalling notations (30) and (35), we arrive at the following approximation for the strains of outer and middle surfaces:

$$\boldsymbol{\varepsilon} = \mathbf{B}^{\mathrm{ANS}}\mathbf{U}, \tag{43}$$

where $\mathbf{B}^{\mathrm{ANS}}$ is the elemental strain–displacement transformation matrix, which is similar to the corresponding matrix $\mathbf{B}$ of the pure displacement-based formulation except for two last rows.

5.3.2. ANS method for in-plane and transverse shear strains. Unfortunately, a conventional ANS method for the transverse shear strains applied to the exact geometry four-node shell element is deficient because membrane locking occurs. This is due to the fact that the exact representation of the reference surface yields the explicit variation of curvatures and Christoffel symbols throughout the element. To circumvent this difficulty, additionally the in-plane strains should be evaluated at five sampling points (Figure 3) and interpolated inside the element by using a usual ANS technique [10]. In our notations the interpolations [10] for covariant components of the strain tensor in the reference surface frame $\tilde{\boldsymbol{a}}^\alpha$, $\tilde{\boldsymbol{a}}^3$ can be written as

$$\begin{aligned} \tilde{\varepsilon}^I_{11} &= \tfrac{1}{2}(1-\xi^2)\tilde{\varepsilon}^I_{11}(B) + \tfrac{1}{2}(1+\xi^2)\tilde{\varepsilon}^I_{11}(D), \\ \tilde{\varepsilon}^I_{22} &= \tfrac{1}{2}(1-\xi^1)\tilde{\varepsilon}^I_{22}(A) + \tfrac{1}{2}(1+\xi^1)\tilde{\varepsilon}^I_{22}(C), \quad \tilde{\varepsilon}^I_{12} = \tilde{\varepsilon}^I_{12}(E). \end{aligned} \tag{44}$$

The transverse shear strains are interpolated throughout the element in a standard form (37). It is important to note that interpolations (37) and (44) have been employed by Roh and Cho [10] for the covariant components of the strain tensor in the frame $\boldsymbol{a}^\alpha$, $\boldsymbol{a}^3$ that simplifies the ANS shell element formulation significantly.

The values of in-plane components of the strain tensor in the natural coordinate system are evaluated at above sampling points by equations

$$2\tilde{\varepsilon}^I_{\alpha\beta} = \tilde{\mu}^{I\gamma}_\beta \left(\frac{\partial \tilde{u}^I_\gamma}{\partial \xi^\alpha} - \tilde{\Gamma}^\delta_{\alpha\gamma}\tilde{u}^I_\delta - \tilde{\Gamma}^3_{\alpha\gamma} w \right) + \tilde{\mu}^{I\gamma}_\alpha \left(\frac{\partial \tilde{u}^I_\gamma}{\partial \xi^\beta} - \tilde{\Gamma}^\delta_{\beta\gamma}\tilde{u}^I_\delta - \tilde{\Gamma}^3_{\beta\gamma} w \right), \tag{45}$$

$$\tilde{\Gamma}^\gamma_{\alpha\beta} = \tilde{\boldsymbol{a}}^\gamma \cdot \frac{\partial \tilde{\boldsymbol{a}}_\alpha}{\partial \xi^\beta} = t^\lambda_\alpha t^\mu_\beta \ell^\gamma_\delta \Gamma^\delta_{\lambda\mu} + (1-\delta_{\alpha\beta})\ell^\gamma_\lambda \eta^\lambda, \tag{46}$$

$$\tilde{\Gamma}^3_{\alpha\beta} = \tilde{\boldsymbol{a}}^3 \cdot \frac{\partial \tilde{\boldsymbol{a}}_\alpha}{\partial \xi^\beta} = t^\lambda_\alpha t^\mu_\beta \Gamma^3_{\lambda\mu}, \quad \eta^\alpha = \frac{\partial^2 \theta^\alpha}{\partial \xi^1 \partial \xi^2} = \frac{1}{4}(\theta^\alpha_1 - \theta^\alpha_2 + \theta^\alpha_3 - \theta^\alpha_4),$$

which follow from relationships (18)–(20), (32) and (38). The components of the shifter tensor at outer surfaces $\tilde{\mu}^{I\beta}_\alpha$ in the natural coordinate system can be found from (41).

Substituting displacement interpolation (31) into strain–displacement equations (37) and (40), (44) and (45), and allowing for tensorial transformations (41), (42) and

$$\varepsilon^I_{\alpha\beta} = \ell^\gamma_\alpha \ell^\delta_\beta \tilde{\varepsilon}^I_{\gamma\delta}, \tag{47}$$

DOI: 10.1002/nme

Table I. Comparison of ANS formulations for the four-node EXG shell element.

Formulation	Membrane plate patch test [20]	Bending plate patch test [20]	Free from shear locking	Free from membrane locking
ANS method for transverse shear strains (Section 5.3.1)	Yes	Yes	Yes	No
ANS method for all strain components (Section 5.3.2)	No	No	Yes	Yes
Enhanced ANS method for all strain components (Section 5.3.3)	Yes	Yes	Yes	Yes

we arrive at the strain approximation (43) with a new strain–displacement transformation matrix $\mathbf{B}^{\mathrm{ANS}}$ of course.

5.3.3. Enhanced ANS method for in-plane and transverse shear strains. As turned out, the ANS interpolations (37) and (44) allow one to overcome shear and membrane locking phenomena efficiently but such a EXG shell element does not pass membrane and bending plate patch tests [20]. To solve this problem, the higher-order terms should be included into the ANS interpolation of in-plane strains throughout the element. A comparison of all ANS methods, which may be employed for development of the four-node EXG shell elements, is listed in Table I.

So, we utilize the enhanced ANS interpolations for in-plane strains of the bottom and top surfaces in the following form:

$$\begin{aligned}
\tilde{\varepsilon}^I_{11} &= \tilde{\varepsilon}^{I00}_{11} + \xi^2 \tilde{\varepsilon}^{I01}_{11} + (\xi^2)^2 \tilde{\varepsilon}^{I02}_{11}, \\
\tilde{\varepsilon}^I_{22} &= \tilde{\varepsilon}^{I00}_{22} + \xi^1 \tilde{\varepsilon}^{I10}_{22} + (\xi^1)^2 \tilde{\varepsilon}^{I20}_{22}, \\
\tilde{\varepsilon}^I_{12} &= \tilde{\varepsilon}^{I00}_{12} + \xi^1 \tilde{\varepsilon}^{I10}_{12} + \xi^2 \tilde{\varepsilon}^{I01}_{12} + \xi^1 \xi^2 \tilde{\varepsilon}^{I11}_{12}.
\end{aligned} \tag{48}$$

Using interpolations (48) in a plate compatibility equation (see e.g. [28]) for in-plane components of the strain tensor in the natural coordinate system

$$\frac{\partial^2 \tilde{\varepsilon}^I_{11}}{\partial \xi^2 \partial \xi^2} - 2\frac{\partial^2 \tilde{\varepsilon}^I_{12}}{\partial \xi^1 \partial \xi^2} + \frac{\partial^2 \tilde{\varepsilon}^I_{22}}{\partial \xi^1 \partial \xi^1} = 2\tilde{\Gamma}^1_{12}\frac{\partial \tilde{\varepsilon}^I_{11}}{\partial \xi^2} + 2\tilde{\Gamma}^2_{12}\frac{\partial \tilde{\varepsilon}^I_{22}}{\partial \xi^1} - 2\tilde{\Gamma}^\alpha_{12}\tilde{\Gamma}^\beta_{12}\tilde{\varepsilon}^I_{\alpha\beta}, \tag{49}$$

where

$$\begin{gathered}
\tilde{\varepsilon}^I_{11} = \frac{\partial \tilde{u}^I_1}{\partial \xi^1}, \quad \tilde{\varepsilon}^I_{22} = \frac{\partial \tilde{u}^I_2}{\partial \xi^2}, \quad 2\tilde{\varepsilon}^I_{12} = \frac{\partial \tilde{u}^I_1}{\partial \xi^2} + \frac{\partial \tilde{u}^I_2}{\partial \xi^1} - 2\tilde{\Gamma}^\alpha_{12}\tilde{u}^I_\alpha, \\
\tilde{\Gamma}^1_{12} = \frac{1}{\Lambda}c_2, \quad \tilde{\Gamma}^2_{12} = \frac{1}{\Lambda}c_1, \quad \Lambda = c_0 + c_\alpha \xi^\alpha,
\end{gathered} \tag{50}$$

one finds

$$\begin{gathered}
\tilde{\varepsilon}^{I02}_{11} = \tilde{\varepsilon}^{I20}_{22} = \tilde{\varepsilon}^{I11}_{12} = \tilde{\varepsilon}^I_*, \quad 2\tilde{\varepsilon}^{I10}_{12} = \tilde{\varepsilon}^{I01}_{11}, \quad 2\tilde{\varepsilon}^{I01}_{12} = \tilde{\varepsilon}^{I10}_{22}, \\
\tilde{\varepsilon}^I_* = \frac{c_2}{c_0}\left(\tilde{\varepsilon}^{I01}_{11} - \frac{c_2}{c_0}\tilde{\varepsilon}^{I00}_{11}\right) + \frac{c_1}{c_0}\left(\tilde{\varepsilon}^{I10}_{22} - \frac{c_1}{c_0}\tilde{\varepsilon}^{I00}_{22}\right) - \frac{2c_1c_2}{c_0^2}\tilde{\varepsilon}^{I00}_{12}.
\end{gathered} \tag{51}$$

DOI: 10.1002/nme

The relations (51) imply that only five approximation modes $\tilde{\varepsilon}_{11}^{I00}$, $\tilde{\varepsilon}_{11}^{I01}$, $\tilde{\varepsilon}_{22}^{I00}$, $\tilde{\varepsilon}_{22}^{I10}$ and $\tilde{\varepsilon}_{12}^{I00}$ for each outer surface are independent of 10 strain approximation modes introduced by (48). This provides a correct rank of the elemental stiffness matrix.

By invoking, as in the previous section, four sampling points A, B, C and D for the in-plane normal strains and one sampling point E for the in-plane shear strain and using strain interpolations (48) in conjunction with (51), the following relations for the independent strain modes are obtained:

$$\begin{aligned}
&\tilde{\varepsilon}_{11}^{I00} = \tfrac{1}{2}[\tilde{\varepsilon}_{11}^{I}(B)+\tilde{\varepsilon}_{11}^{I}(D)]-\tilde{\varepsilon}_{*}^{I}, \quad \tilde{\varepsilon}_{11}^{I01} = \tfrac{1}{2}[\tilde{\varepsilon}_{11}^{I}(D)-\tilde{\varepsilon}_{11}^{I}(B)],\\
&\tilde{\varepsilon}_{22}^{I00} = \tfrac{1}{2}[\tilde{\varepsilon}_{22}^{I}(A)+\tilde{\varepsilon}_{22}^{I}(C)]-\tilde{\varepsilon}_{*}^{I}, \quad \tilde{\varepsilon}_{22}^{I10} = \tfrac{1}{2}[\tilde{\varepsilon}_{22}^{I}(C)-\tilde{\varepsilon}_{22}^{I}(A)], \quad \tilde{\varepsilon}_{12}^{I00} = \tilde{\varepsilon}_{12}^{I}(E).
\end{aligned} \tag{52}$$

The use of relations (51) and (52) in (48) leads to a final form of the enhanced ANS interpolations for in-plane strain components

$$\begin{aligned}
\tilde{\varepsilon}_{11}^{I} &= \tfrac{1}{2}(1-\xi^2)\tilde{\varepsilon}_{11}^{I}(B)+\tfrac{1}{2}(1+\xi^2)\tilde{\varepsilon}_{11}^{I}(D)-[1-(\xi^2)^2]\tilde{\varepsilon}_{*}^{I},\\
\tilde{\varepsilon}_{22}^{I} &= \tfrac{1}{2}(1-\xi^1)\tilde{\varepsilon}_{22}^{I}(A)+\tfrac{1}{2}(1+\xi^1)\tilde{\varepsilon}_{22}^{I}(C)-[1-(\xi^1)^2]\tilde{\varepsilon}_{*}^{I},\\
\tilde{\varepsilon}_{12}^{I} &= \tilde{\varepsilon}_{12}^{I}(E)+\tfrac{1}{4}\xi^1[\tilde{\varepsilon}_{11}^{I}(D)-\tilde{\varepsilon}_{11}^{I}(B)]+\tfrac{1}{4}\xi^2[\tilde{\varepsilon}_{22}^{I}(C)-\tilde{\varepsilon}_{22}^{I}(A)]+\xi^1\xi^2\tilde{\varepsilon}_{*}^{I}
\end{aligned} \tag{53}$$

with a new presentation of the higher-order strain modes

$$\begin{aligned}
\tilde{\varepsilon}_{*}^{I} = &-\frac{c_2(c_0+c_2)}{2d}\tilde{\varepsilon}_{11}^{I}(B)+\frac{c_2(c_0-c_2)}{2d}\tilde{\varepsilon}_{11}^{I}(D)\\
&-\frac{c_1(c_0+c_1)}{2d}\tilde{\varepsilon}_{22}^{I}(A)+\frac{c_1(c_0-c_1)}{2d}\tilde{\varepsilon}_{22}^{I}(C)-\frac{2c_1c_2}{d}\tilde{\varepsilon}_{12}^{I}(E),
\end{aligned} \tag{54}$$

where $d = c_0^2 - c_1^2 - c_2^2$.

Inserting the displacement interpolation (31) into strain–displacement equations (37) and (40), (53) and (45), taking into account tensorial transformations (41), (42) and (47), and recalling notations (30) and (35), we arrive again at the strain interpolation (43).

5.4. Elemental stiffness matrix of ANS four-node EXG shell element

Using interpolations (31) and (43) in the displacement-based variational equation (29) and allowing for coordinate transformation (32), one derives the element equilibrium equations

$$\mathbf{KU} = \mathbf{F}, \tag{55}$$

where $\mathbf{K}$ is the elemental stiffness matrix and $\mathbf{F}$ is the force vector given by

$$\begin{aligned}
&\mathbf{K} = \int\!\!\int_{\tilde{\Omega}_{\mathrm{el}}} (\mathbf{B}^{\mathrm{ANS}})^{\mathrm{T}}\mathbf{D}\mathbf{B}^{\mathrm{ANS}}\sqrt{a}\Lambda\,\mathrm{d}\xi^1\,\mathrm{d}\xi^2,\\
&\mathbf{F} = [-F_{-1}^1 \;\; -F_{-1}^2 \;\; (-F_{-1}^3+F_{+1}^3) \;\; F_{+1}^1 \;\; F_{+1}^2 \;\; \ldots \;\; -F_{-4}^1 \;\; -F_{-4}^2 \;\; (-F_{-4}^3+F_{+4}^3) \;\; F_{+4}^1 \;\; F_{+4}^2]^{\mathrm{T}},\\
&F_{Ir}^{i} = \int\!\!\int_{\tilde{\Omega}_{\mathrm{el}}} \mu^I p_I^i N_r \sqrt{a}\Lambda\,\mathrm{d}\xi^1\,\mathrm{d}\xi^2 \qquad \text{(no summation is needed).}
\end{aligned} \tag{56}$$

DOI: 10.1002/nme

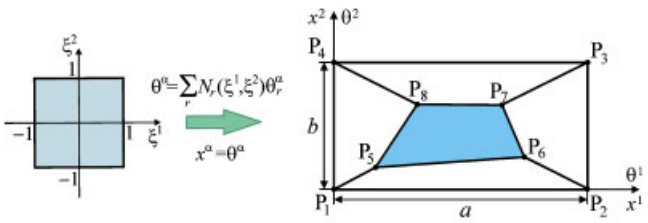

Coordinate	P_5	P_6	P_7	P_8
θ^1	4	18	16	8
θ^2	2	3	8	8

$a = 24,\ b = 12,\ h = 0.1$

$E = 10^6,\ \nu = 0.25,\ e = 10^{-5}$

Figure 4. Plate patch test.

Remark 5

Here and in the following studies, the integrals are calculated by employing the Gauss integration scheme with 2×2 integration points. In this aspect, we mention that the stiffness matrix $\mathbf{K}$, corresponding to each ANS method from Sections 5.3.2 and 5.3.3, has six zero eigenvalues as required for satisfaction of the general rigid-body motion representation.

5.5. Patch tests

The plate patch tests for the membrane behavior and out of plane bending behavior of shell elements confirm that the finite element formulation developed is able to reproduce constant stress–strain states for distorted mesh configurations. Here, we consider a patch of five plate elements [20] with four external and four internal nodes as depicted in Figure 4.

5.5.1. Membrane patch test. The displacements of the bottom and top planes at exterior nodes are prescribed as follows:

$$u_1^I = e\left(\theta^1 + \frac{1}{2}\theta^2\right), \quad u_2^I = e\left(\frac{1}{2}\theta^1 + \theta^2\right), \quad w = 0. \tag{57}$$

Such a displacement distribution yields a constant in-plane strain field, that is,

$$\varepsilon_{\alpha\alpha}^I = e, \quad 2\varepsilon_{12}^I = e, \quad \varepsilon_{\alpha 3}^M = 0. \tag{58}$$

The numerical results show that both EXG shell elements, based on the ANS interpolations from Sections 5.3.1 and 5.3.3, pass the membrane plate patch test. In regards to a shell element based on the ANS interpolation from Section 5.3.2, the computed displacements and strains at the interior nodes do not agree well with exact ones (57) and (58).

5.5.2. Bending patch test. To achieve a constant bending stress–strain state, the displacements of outer planes can be chosen as

$$u_1^\pm = \mp e\left(\theta^1 + \frac{1}{2}\theta^2\right), \quad u_2^\pm = \mp e\left(\frac{1}{2}\theta^1 + \theta^2\right), \quad w = \frac{1}{h}e\left[(\theta^1)^2 + \theta^1\theta^2 + (\theta^2)^2\right]. \tag{59}$$

DOI: 10.1002/nme

Table II. Displacements at interior nodes in the bending plate patch test.

Formulation	Node	u_1^-	u_2^-	w
ANS method	P_5	5.0000044×10^{-5}	4.0000037×10^{-5}	2.8000025×10^{-3}
for transverse	P_6	1.9499995×10^{-4}	1.1999998×10^{-4}	3.8700002×10^{-2}
shear strains	P_7	1.9999997×10^{-4}	1.5999999×10^{-4}	4.4800003×10^{-2}
	P_8	1.2000002×10^{-4}	1.1999994×10^{-4}	1.9200004×10^{-2}
ANS method	P_5	2.7517076×10^{-5}	6.4498797×10^{-5}	1.8921260×10^{-4}
for all strain	P_6	2.5920596×10^{-4}	1.0110405×10^{-4}	3.4280788×10^{-2}
components	P_7	3.3539259×10^{-4}	1.4361476×10^{-4}	3.4624385×10^{-2}
	P_8	1.4097688×10^{-5}	1.0877357×10^{-4}	8.9210119×10^{-3}
Enhanced	P_5	5.0000044×10^{-5}	4.0000037×10^{-5}	2.8000025×10^{-3}
ANS method	P_6	1.9499995×10^{-4}	1.1999998×10^{-4}	3.8700002×10^{-2}
for all strain	P_7	1.9999997×10^{-4}	1.5999999×10^{-4}	4.4800003×10^{-2}
components	P_8	1.2000002×10^{-4}	1.1999994×10^{-4}	1.9200004×10^{-2}

The use of displacement distributions (59) in strain–displacement equations (20) leads to

$$\varepsilon_{\alpha\alpha}^{\pm}=\mp e,\quad 2\varepsilon_{12}^{\pm}=\mp e,\quad \varepsilon_{\alpha3}^{M}=0. \tag{60}$$

It should be noticed that in the case of zero surface tractions the equilibrium equations of the plate are fulfilled in a strong sense.

Applying the prescribed displacements to exterior nodes, one can see that displacements and strains at interior nodes are exactly identical to the analytical answers (59) and (60) for the above ANS elements from Sections 5.3.1 and 5.3.3. The ANS element from Section 5.3.2 does not pass again the patch test. The calculated displacements at interior nodes are listed in Table II. Note that all computations were performed on a PC Pentium IV by using Delphi environment.

6. HYBRID ANS FOUR-NODE EXG SHELL ELEMENTS

To improve the computational efficiency of the ANS four-node shell elements, a hybrid method may be employed. In the present paper, the hybrid method stands for the one, which is formulated by applying mixed variational principles but the governing elemental equations consist of only the nodal displacements as unknowns [23].

6.1. Hybrid stress method

The hybrid stress finite element formulation is based on the Hellinger–Reissner variational principle [28], which can be expressed in our notations (22) and (30) as

$$\iint_{\bar{\Omega}_{\mathrm{el}}}[\delta\mathbf{H}^{\mathrm{T}}(\boldsymbol{\varepsilon}-\mathbf{D}^{-1}\mathbf{H})+\delta\boldsymbol{\varepsilon}^{\mathrm{T}}\mathbf{H}-\delta\mathbf{v}^{\mathrm{T}}\mathbf{p}]\sqrt{a}\,\mathrm{d}\theta^1\,\mathrm{d}\theta^2-\delta\overset{\smile}{W}{}_{\mathrm{el}}^{\mathrm{ext}}=0, \tag{61}$$

where $\mathbf{H}$ is the stress resultant vector given by

$$\mathbf{H}=[H_-^{11}\ \ H_+^{11}\ \ H_-^{22}\ \ H_+^{22}\ \ H_-^{12}\ \ H_+^{12}\ \ H^{13}\ \ H^{23}]^{\mathrm{T}}. \tag{62}$$

DOI: 10.1002/nme

We refer to (61) as a Hellinger–Reissner variational equation. A short discussion on that is presented in Appendix A.

In order to fulfill a patch test, the assumed stress resultants are interpolated throughout the element as follows [22, 29]:

$$\mathbf{H}=\mathbf{P}_H\boldsymbol{\psi},\quad \boldsymbol{\psi}=[\psi_1\quad \psi_2\ldots\psi_{14}]^{\mathrm{T}},\quad \mathbf{P}_H=[\mathbf{I}_8\quad \bar{\mathbf{P}}_H],$$

$$\bar{\mathbf{P}}_H=\begin{bmatrix} \bar{t}_1^1\bar{t}_1^1\bar{\xi}^2 & 0 & \bar{t}_2^1\bar{t}_2^1\bar{\xi}^1 & 0 & 0 & 0\\ 0 & \bar{t}_1^1\bar{t}_1^1\bar{\xi}^2 & 0 & \bar{t}_2^1\bar{t}_2^1\bar{\xi}^1 & 0 & 0\\ \bar{t}_1^2\bar{t}_1^2\bar{\xi}^2 & 0 & \bar{t}_2^2\bar{t}_2^2\bar{\xi}^1 & 0 & 0 & 0\\ 0 & \bar{t}_1^2\bar{t}_1^2\bar{\xi}^2 & 0 & \bar{t}_2^2\bar{t}_2^2\bar{\xi}^1 & 0 & 0\\ \bar{t}_1^1\bar{t}_1^2\bar{\xi}^2 & 0 & \bar{t}_2^1\bar{t}_2^2\bar{\xi}^1 & 0 & 0 & 0\\ 0 & \bar{t}_1^1\bar{t}_1^2\bar{\xi}^2 & 0 & \bar{t}_2^1\bar{t}_2^2\bar{\xi}^1 & 0 & 0\\ 0 & 0 & 0 & 0 & \bar{t}_1^1\bar{\xi}^2 & \bar{t}_2^1\bar{\xi}^1\\ 0 & 0 & 0 & 0 & \bar{t}_1^2\bar{\xi}^2 & \bar{t}_2^2\bar{\xi}^1 \end{bmatrix}, \tag{63}$$

where $\mathbf{I}_8$ is the unit matrix of order 8×8; $\bar{t}_\alpha^\beta$ are the elements of the Jacobian transformation matrix (33) evaluated at the element center; $\bar{\xi}^\alpha=\xi^\alpha-\xi_c^\alpha$ are the transformed natural coordinates defined as

$$\begin{aligned} &\bar{t}_1^\alpha=\tfrac{1}{4}(\theta_1^\alpha-\theta_2^\alpha-\theta_3^\alpha+\theta_4^\alpha),\qquad \bar{t}_2^\alpha=\tfrac{1}{4}(\theta_1^\alpha+\theta_2^\alpha-\theta_3^\alpha-\theta_4^\alpha),\\ &\xi_c^\alpha=\frac{1}{A_{\mathrm{el}}}\int\!\!\int_{\tilde{\Omega}_{\mathrm{el}}}\xi^\alpha\sqrt{a}\Lambda\,\mathrm{d}\xi^1\,\mathrm{d}\xi^2,\quad A_{\mathrm{el}}=\int\!\!\int_{\tilde{\Omega}_{\mathrm{el}}}\sqrt{a}\Lambda\,\mathrm{d}\xi^1\,\mathrm{d}\xi^2. \end{aligned} \tag{64}$$

The purpose of introducing $\bar{\xi}^\alpha$ lies in the simplicity of some elemental matrices of the hybrid method because a useful formula

$$\int\!\!\int_{\tilde{\Omega}_{\mathrm{el}}}\bar{\xi}^\alpha\sqrt{a}\Lambda\,\mathrm{d}\xi^1\,\mathrm{d}\xi^2=0$$

holds.

The use of interpolations (31), (32), (43) and (63) in the mixed variational equation (61) leads to equilibrium equations

$$\mathbf{R}_H\mathbf{U}=\mathbf{G}_H\boldsymbol{\psi},\quad \mathbf{R}_H^{\mathrm{T}}\boldsymbol{\psi}=\mathbf{F}, \tag{65}$$

where

$$\mathbf{G}_H=\int\!\!\int_{\tilde{\Omega}_{\mathrm{el}}}\mathbf{P}_H^{\mathrm{T}}\mathbf{D}^{-1}\mathbf{P}_H\sqrt{a}\Lambda\,\mathrm{d}\xi^1\,\mathrm{d}\xi^2,\quad \mathbf{R}_H=\int\!\!\int_{\tilde{\Omega}_{\mathrm{el}}}\mathbf{P}_H^{\mathrm{T}}\mathbf{B}^{\mathrm{ANS}}\sqrt{a}\Lambda\,\mathrm{d}\xi^1\,\mathrm{d}\xi^2. \tag{66}$$

DOI: 10.1002/nme

Owing to the fact that stress resultants (63) are interpolated discontinuously across element boundaries, the assumed stress parameter vector $\boldsymbol{\psi}$ can be eliminated at the element level, and we arrive at the pure displacement-based problem

$$\mathbf{K}_H\mathbf{U}=\mathbf{F}, \tag{67}$$

where $\mathbf{K}_H$ denotes the element stiffness matrix given by

$$\mathbf{K}_H=\mathbf{R}_H^{\mathrm{T}}\mathbf{G}_H^{-1}\mathbf{R}_H. \tag{68}$$

It is seen that the hybrid stress shell element formulation requires a numerical inversion of the matrix of order 14×14.

6.2. *Hybrid strain method*

The hybrid strain finite element formulation is based on the modified Hellinger–Reissner functional [24], in which displacements and strains are utilized as fundamental shell unknowns. Therefore, taking into account the distribution of displacement-dependent strains through the thickness of the shell (14) and using constitutive equations (25) and matrix notations (30) into the above 3D mixed functional, we represent the 2D modified Hellinger–Reissner variational equation in the following form:

$$\int\!\!\int_{\bar{\Omega}_{\mathrm{el}}}[\delta\mathbf{E}^{\mathrm{T}}\mathbf{D}(\boldsymbol{\varepsilon}-\mathbf{E})+\delta\boldsymbol{\varepsilon}^{\mathrm{T}}\mathbf{D}\mathbf{E}-\delta\mathbf{v}^{\mathrm{T}}\mathbf{p}]\sqrt{a}\,\mathrm{d}\theta^1\,\mathrm{d}\theta^2-\delta\breve{W}_{\mathrm{el}}^{\mathrm{ext}}=0. \tag{69}$$

Here, $\mathbf{E}$ is the assumed strain vector defined as

$$\mathbf{E}=[E_{11}^{-}\;E_{11}^{+}\;E_{22}^{-}\;E_{22}^{+}\;2E_{12}^{-}\;2E_{12}^{-}\;2E_{13}\;2E_{23}]^{\mathrm{T}}, \tag{70}$$

where $E_{\alpha\beta}^{I}$ and $E_{\alpha 3}$ denote displacement-independent in-plane strains of the bottom and top surfaces and transverse shear strains of the midsurface.

To fulfill a patch test, the displacement-independent strains are interpolated throughout the element as follows:

$$\mathbf{E}=\mathbf{P}_E\boldsymbol{\varphi},\quad \boldsymbol{\varphi}=[\varphi_1\quad\varphi_2\quad\ldots\quad\varphi_{14}]^{\mathrm{T}},\quad \mathbf{P}_E=[\mathbf{I}_8\quad\bar{\mathbf{P}}_E],$$

$$\bar{\mathbf{P}}_E=\begin{bmatrix}
\bar{\ell}_1^1\bar{\ell}_1^1\bar{\xi}^2 & 0 & \bar{\ell}_1^2\bar{\ell}_1^2\bar{\xi}^1 & 0 & 0 & 0\\
0 & \bar{\ell}_1^1\bar{\ell}_1^1\bar{\xi}^2 & 0 & \bar{\ell}_1^2\bar{\ell}_1^2\bar{\xi}^1 & 0 & 0\\
\bar{\ell}_2^1\bar{\ell}_2^1\bar{\xi}^2 & 0 & \bar{\ell}_2^2\bar{\ell}_2^2\bar{\xi}^1 & 0 & 0 & 0\\
0 & \bar{\ell}_2^1\bar{\ell}_2^1\bar{\xi}^2 & 0 & \bar{\ell}_2^2\bar{\ell}_2^2\bar{\xi}^1 & 0 & 0\\
2\bar{\ell}_1^1\bar{\ell}_2^1\bar{\xi}^2 & 0 & 2\bar{\ell}_1^2\bar{\ell}_2^2\bar{\xi}^1 & 0 & 0 & 0\\
0 & 2\bar{\ell}_1^1\bar{\ell}_2^1\bar{\xi}^2 & 0 & 2\bar{\ell}_1^2\bar{\ell}_2^2\bar{\xi}^1 & 0 & 0\\
0 & 0 & 0 & 0 & \bar{\ell}_1^1\bar{\xi}^2 & \bar{\ell}_1^2\bar{\xi}^1\\
0 & 0 & 0 & 0 & \bar{\ell}_2^1\bar{\xi}^2 & \bar{\ell}_2^2\bar{\xi}^1
\end{bmatrix}. \tag{71}$$

DOI: 10.1002/nme

that corresponds to the interpolation of stress resultants (63), where $\bar{\ell}_\alpha^\beta$ are the elements of the inverse Jacobian transformation matrix evaluated at the element center as

$$\bar{\ell}_1^1=\frac{1}{c_0}\bar{t}_2^2,\quad \bar{\ell}_1^2=-\frac{1}{c_0}\bar{t}_1^2,\quad \bar{\ell}_2^1=-\frac{1}{c_0}\bar{t}_2^1,\quad \bar{\ell}_2^2=\frac{1}{c_0}\bar{t}_1^1. \tag{72}$$

Substituting interpolations (31), (32), (43) and (71) in the mixed variational equation (69), we derive the elemental equilibrium equations

$$\mathbf{R}_E\mathbf{U}=\mathbf{G}_E\boldsymbol{\varphi},\quad \mathbf{R}_E^{\mathrm{T}}\boldsymbol{\varphi}=\mathbf{F}, \tag{73}$$

where

$$\mathbf{G}_E=\int\!\!\int_{\tilde{\Omega}_{\mathrm{el}}}\mathbf{P}_E^{\mathrm{T}}\mathbf{D}\mathbf{P}_E\sqrt{a}\Lambda\,\mathrm{d}\xi^1\,\mathrm{d}\xi^2,\quad \mathbf{R}_E=\int\!\!\int_{\tilde{\Omega}_{\mathrm{el}}}\mathbf{P}_E^{\mathrm{T}}\mathbf{D}\mathbf{B}^{\mathrm{ANS}}\sqrt{a}\Lambda\,\mathrm{d}\xi^1\,\mathrm{d}\xi^2. \tag{74}$$

Since the assumed strain interpolations (71) are discontinuous at the element boundaries, the elimination on the element level yields the element stiffness matrix

$$\mathbf{K}_E=\mathbf{R}_E^{\mathrm{T}}\mathbf{G}_E^{-1}\mathbf{R}_E. \tag{75}$$

Thus, again a pure displacement-based problem

$$\mathbf{K}_E\mathbf{U}=\mathbf{F} \tag{76}$$

has to be solved.

One can see that the hybrid strain shell element formulation also leads to the numerical inversion of the matrix of order 14×14.

6.3. Hybrid stress–strain method

To develop the hybrid stress–strain finite element formulation, we have to invoke the Hu–Washizu variational principal in which displacements, strains and stresses are utilized as independent variables. Inserting distributions of displacements, displacement-dependent and displacement-independent strains through the thickness of the shell into the 3D Hu–Washizu functional [28] and taking into account notations (30), (62) and (70), one finds

$$\int\!\!\int_{\tilde{\Omega}_{\mathrm{el}}}[\delta\mathbf{E}^{\mathrm{T}}(\mathbf{D}\mathbf{E}-\mathbf{H})+\delta\mathbf{H}^{\mathrm{T}}(\boldsymbol{\varepsilon}-\mathbf{E})+\delta\boldsymbol{\varepsilon}^{\mathrm{T}}\mathbf{H}-\delta\mathbf{v}^{\mathrm{T}}\mathbf{p}]\sqrt{a}\,\mathrm{d}\theta^1\,\mathrm{d}\theta^2-\delta\breve{W}_{\mathrm{el}}^{\mathrm{ext}}=0. \tag{77}$$

We refer to (77) as a Hu–Washizu variational equation (see Appendix A).

Using all interpolations introduced, namely, (31), (32), (43), (63) and (71) in the variational equation (77), the following equilibrium equations are obtained:

$$\mathbf{Q}^{\mathrm{T}}\boldsymbol{\psi}=\mathbf{G}_E\boldsymbol{\varphi},\quad \mathbf{Q}\boldsymbol{\varphi}=\mathbf{R}_H\mathbf{U},\quad \mathbf{R}_H^{\mathrm{T}}\boldsymbol{\psi}=\mathbf{F}, \tag{78}$$

where

$$\mathbf{Q}=\int\!\!\int_{\tilde{\Omega}_{\mathrm{el}}}\mathbf{P}_H^{\mathrm{T}}\mathbf{P}_E\sqrt{a}\Lambda\,\mathrm{d}\xi^1\,\mathrm{d}\xi^2. \tag{79}$$

DOI: 10.1002/nme

The use of transformed natural coordinates $\bar{\xi}^{\alpha}$ in formulas (63) and (71) for matrices $\bar{\mathbf{P}}_H$ and $\bar{\mathbf{P}}_E$ is of great importance, since a basic matrix of the hybrid stress–strain method $\mathbf{Q}$ becomes diagonal, that is,

$$\mathbf{Q}=\boldsymbol{A}_{\mathrm{el}}\ \mathrm{diag}[\mathbf{I}_8,\omega_2,\omega_2,\omega_1,\omega_1,\omega_2,\omega_1], \tag{80}$$

where

$$\omega_{\alpha}=\frac{1}{\boldsymbol{A}_{\mathrm{el}}}\int\!\!\int_{\tilde{\Omega}_{\mathrm{el}}}(\xi^{\alpha})^2\sqrt{a}\Lambda\,\mathrm{d}\xi^1\,\mathrm{d}\xi^2-(\xi_c^{\alpha})^2.$$

Eliminating assumed stress and strain parameter vectors $\boldsymbol{\psi}$ and $\boldsymbol{\varphi}$ from elemental equations (78), we arrive at the governing equations

$$\mathbf{K}_{EH}\mathbf{U}=\mathbf{F}, \tag{81}$$

where $\mathbf{K}_{EH}$ denotes the element stiffness matrix given by

$$\mathbf{K}_{EH}=\mathbf{R}_H^{\mathrm{T}}\mathbf{Q}^{-1}\mathbf{G}_E\mathbf{Q}^{-1}\mathbf{R}_H \tag{82}$$

Because of a simple structure of the matrix $\mathbf{Q}$, its inversion can be readily fulfilled in a closed form

$$\mathbf{Q}^{-1}=\frac{1}{\boldsymbol{A}_{\mathrm{el}}}\ \mathrm{diag}\left[\mathbf{I}_8,\frac{1}{\omega_2},\frac{1}{\omega_2},\frac{1}{\omega_1},\frac{1}{\omega_1},\frac{1}{\omega_2},\frac{1}{\omega_1}\right].$$

Thus, no expensive numerical inversion is needed if one uses the hybrid stress–strain method in the framework of the EXG shell element formulation developed.

7. NUMERICAL EXAMPLES

The performance of the proposed four-node EXG shell elements is evaluated with several problems extracted from the literature. A listing of these elements and the abbreviations used to identify them are contained in Table III.

Table III. Listing of four-node shell elements.

Name	Description
EXG4A	Exact geometry shell element based on the enhanced ANS method for in-plane and transverse shear strains (Section 5.3.3)
EXG4Aσ	EXG4A element on the basis of the hybrid stress method (Section 6.1)
EXG4Aε	EXG4A element on the basis of the hybrid strain method (Section 6.2)
EXG4A$\sigma\varepsilon$	EXG4A element on the basis of the hybrid stress–strain method (Section 6.3)
ISO4SRI	Isoparametric degenerated shell element with selective reduced integration [30]
ISO4URI	Isoparametric degenerated shell element with uniform reduced integration and stabilization [31]
ISO4A	Isoparametric degenerated ANS shell element (MITC4) [19]
ISOP4A	Isoparametric ANS plate element [16]
ISO4Aσ	Isoparametric ANS shell element on the basis of the hybrid stress method [29]

DOI: 10.1002/nme

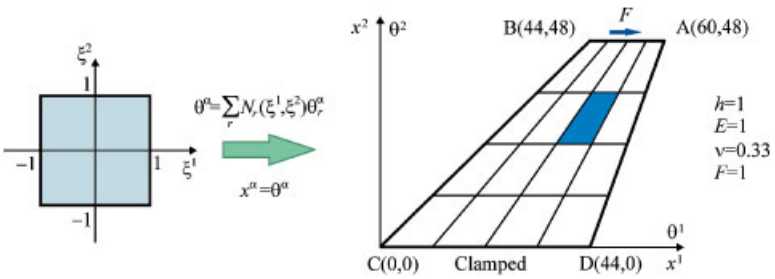

Figure 5. Cook's membrane problem—a plate element formulation.

Table IV. Normalized in-plane tip displacement of the trapezoidal plate—a plate element formulation.

Mesh	EXG4A	EXG4Aσ	EXG4Aε	EXG4A$\sigma\varepsilon$	ISO4Aσ
2×2	0.4954	0.8835	0.5555	0.7332	0.883
4×4	0.7654	0.9627	0.8120	0.9126	0.963
8×8	0.9234	0.9906	0.9421	0.9760	0.991
16×16	0.9798	0.9987	0.9853	0.9948	0.999

7.1. Cantilever trapezoidal plate (Cook's membrane problem)

A trapezoidal plate is clamped on one side, whereas the opposite side is subjected to a distributed in-plane load [29]. This test is an excellent ability to verify a proper representation of the membrane dominated stress state with skewed meshes.

7.1.1. Cook's membrane problem and plate element formulation. Consideration of the Cook's membrane problem, as shown in Figure 5, corresponds to the standard isoparametric plate element formulation and has been carried out by many researches. Herein, we repeat this finite element technique because the geometric objects of the problem are

$$\Gamma^{i}_{\alpha\beta}=0, \quad b^{\alpha}_{\beta}=0, \quad m^{\alpha}_{\beta}=\delta^{\alpha}_{\beta}, \quad \sqrt{a}=1. \tag{83}$$

Table IV lists the normalized in-plane tip displacement of the midplane and a comparison with results of Simo *et al.* [29]. For this purpose a converged finite element solution of 23.91 has been used. As turned out, a hybrid strain ANS shell element finished with the lowest rank among all hybrid EXG elements developed. It is also seen that both hybrid stress ANS elements EXG4Aσ and ISO4Aσ yield practically the same results.

7.1.2. Cook's membrane problem and shell element formulation. Let us consider a trapezoidal plate displayed in Figure 6. It is apparent, in this case we deal with a flat shell, since a specific transform $x^{\alpha}=x^{\alpha}(\theta^1,\theta^2)$ given in Figure 6 maps a biunit square in (θ^1,θ^2)-space into a trapezium

DOI: 10.1002/nme

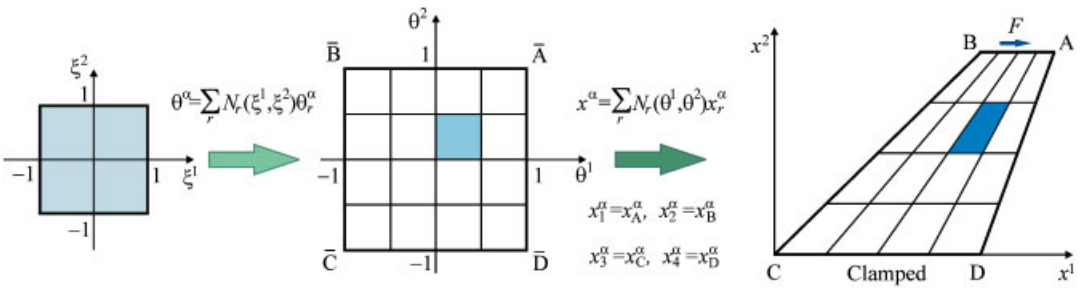

Figure 6. Cook's membrane problem—a shell element formulation.

Table V. Normalized in-plane tip displacement of the trapezoidal plate—a shell element formulation.

Mesh	EXG4A	EXG4Aσ	EXG4Aε	EXG4A$\sigma\varepsilon$
2×2	0.6337	1.0574	0.8079	0.8671
4×4	0.8186	1.0146	0.8935	0.9560
8×8	0.9393	1.0036	0.9650	0.9877
16×16	0.9840	1.0019	0.9912	0.9978

ABCD in (x^1, x^2)-space, where $x^\alpha_{\rm A}$, $x^\alpha_{\rm B}$, $x^\alpha_{\rm C}$ and $x^\alpha_{\rm D}$ are the Cartesian coordinates of points A, B, C and D. Therefore, we have the following geometric quantities:

$$
\begin{aligned}
&\Gamma^\alpha_{12}=\widehat{\eta}^1\widehat{\ell}^\alpha_1+\widehat{\eta}^2\widehat{\ell}^\alpha_2, \quad \Gamma^\alpha_{\beta\beta}=\Gamma^3_{\alpha\beta}=0, \quad b^\alpha_\beta=0, \quad \sqrt{a}=\widehat{\Lambda},\\
&\widehat{t}^\alpha_1=\frac{\partial x^\alpha}{\partial\theta^1}=\frac{1}{4}(1+\theta^2)(x^\alpha_{\rm A}-x^\alpha_{\rm B})+\frac{1}{4}(1-\theta^2)(x^\alpha_{\rm D}-x^\alpha_{\rm C}),\\
&\widehat{t}^\alpha_2=\frac{\partial x^\alpha}{\partial\theta^2}=\frac{1}{4}(1+\theta^1)(x^\alpha_{\rm A}-x^\alpha_{\rm D})+\frac{1}{4}(1-\theta^1)(x^\alpha_{\rm B}-x^\alpha_{\rm C}),\\
&\widehat{\eta}^\alpha=\frac{\partial^2 x^\alpha}{\partial\theta^1\partial\theta^2}=\frac{1}{4}(x^\alpha_{\rm A}-x^\alpha_{\rm B}+x^\alpha_{\rm C}-x^\alpha_{\rm D}), \quad m^\alpha_\beta=\widehat{\ell}^\alpha_\beta=\frac{\partial\theta^\alpha}{\partial x^\beta},\\
&\widehat{\ell}^1_1=\frac{1}{\widehat{\Lambda}}\widehat{t}^2_2, \quad \widehat{\ell}^2_1=-\frac{1}{\widehat{\Lambda}}\widehat{t}^2_1, \quad \widehat{\ell}^1_2=-\frac{1}{\widehat{\Lambda}}\widehat{t}^1_2, \quad \widehat{\ell}^2_2=\frac{1}{\widehat{\Lambda}}\widehat{t}^1_1, \quad \widehat{\Lambda}=\det[\widehat{t}^\alpha_\beta].
\end{aligned}
\tag{84}
$$

One can compare corresponding equations in (83) and (84) with each other.

Table V lists results of the convergence study. It is seen that in the case of coarse meshes the results derived are much better than corresponding ones from Table IV. Note that again a hybrid stress ANS element EXG4Aσ performs excellently and its performance is among the ranks of the best isoparametric nine-node plate/shell elements.

7.2. Simply supported square plate under central load

This problem has been selected to test the effect of mesh distortion on the performance of the proposed four-node EXG shell elements. Owing to symmetry, one quarter of the simply supported

DOI: 10.1002/nme

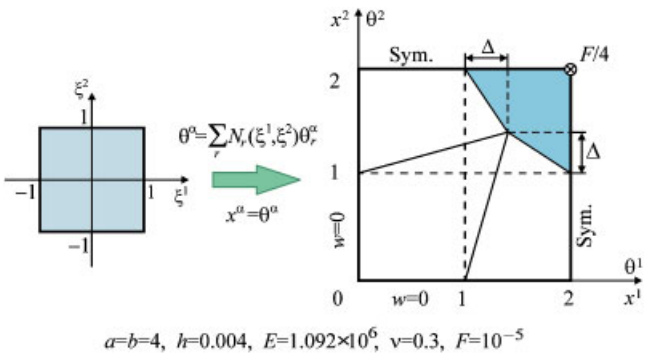

Figure 7. Simply supported square plate with a distorted 2×2 mesh.

Table VI. Normalized transverse center point displacement of the square plate.

Δ	EXG4A	EXG4Aσ	EXG4Aε	EXG4Aσε	ISO4Aσ	ISOP4A*
0.0	0.9922	1.0074	1.0042	1.0042	1.002	0.991
0.1	0.9871	1.0026	0.9985	0.9990	0.998	0.986
0.2	0.9768	0.9917	0.9886	0.9871	0.988	0.976
0.3	0.9608	0.9739	0.9739	0.9676	0.972	0.961
0.4	0.9378	0.9483	0.9535	0.9395	0.949	0.939
0.5	0.9048	0.9139	0.9257	0.9007	0.918	0.907
0.6	0.8511	0.8697	0.8865	0.8480	0.879	0.858

*Results were obtained by Simo *et al.* [29].

square plate subjected to a concentrated load at the center point is modeled by a very coarse 2×2 mesh. The geometrical and mechanical data of the problem are displayed in Figure 7. The mesh is distorted by moving the inner node along the diagonal of the upper right square.

Table VI lists the transverse central displacement normalized with respect to the analytical solution [32] of $0.01160\,Fa^2/D$, which is based on the Kirchhoff plate theory. It is seen that all ANS shell elements perform very well even in the case of the extremely large values of the distortion parameter Δ.

To investigate the performance of the ANS displacement-based element EXG4A more carefully, we consider the distorted $4n\times 4n$ element meshes, as shown in Figure 8, generated by $2n\times 2n$ squares with above distorted 2×2 meshes (Figure 7). The distortion parameter for each mesh configuration can be found through a simple formula $d_n=\Delta/2n$, whereas the distortion parameter Δ varies again in a range of $0\leqslant\Delta\leqslant 0.6$. Figure 9 presents the results of the convergence study due to mesh refinement and mesh distortion. As can be seen, the EXG4A element behaves practically insensitive with respect to extremely high mesh distortion.

7.3. Pinched cylindrical shell with rigid diaphragms

To illustrate the capability of the proposed four-node EXG shell elements to overcome shear and membrane locking phenomena (shear locking is much greater than membrane locking [33]) and to compare it with high-performance isoparametric four-node shell elements [19, 29–31],

DOI: 10.1002/nme

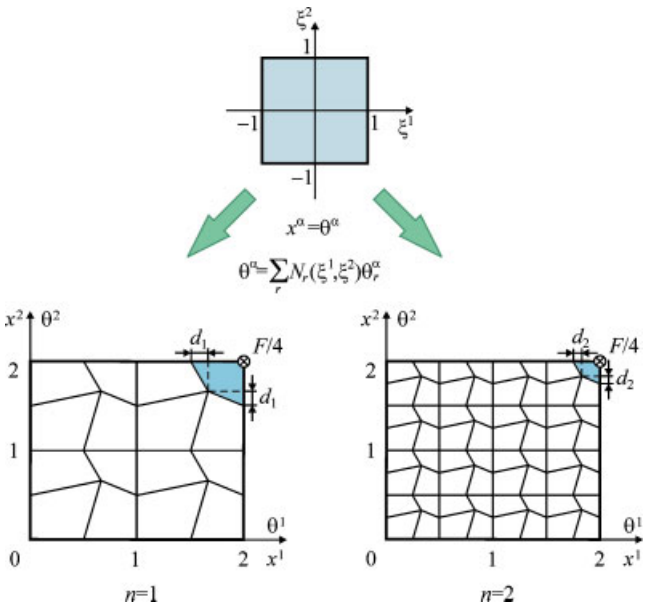

Figure 8. Simply supported square plate with distorted $4n \times 4n$ meshes, where the distortion parameter $d_n = \Delta/2n$ $(n = 1, 2, \ldots, 10; \Delta \in [0, 0.6])$.

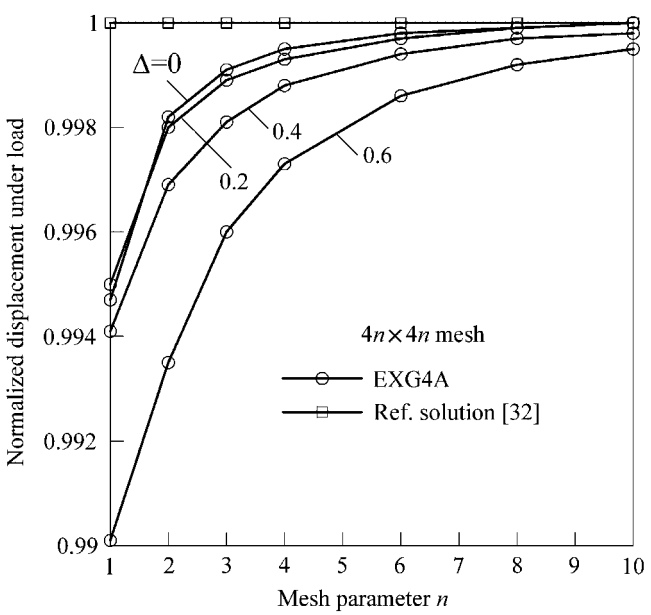

Figure 9. Convergence study due to mesh refinement and mesh distortion for a simply supported square plate.

DOI: 10.1002/nme

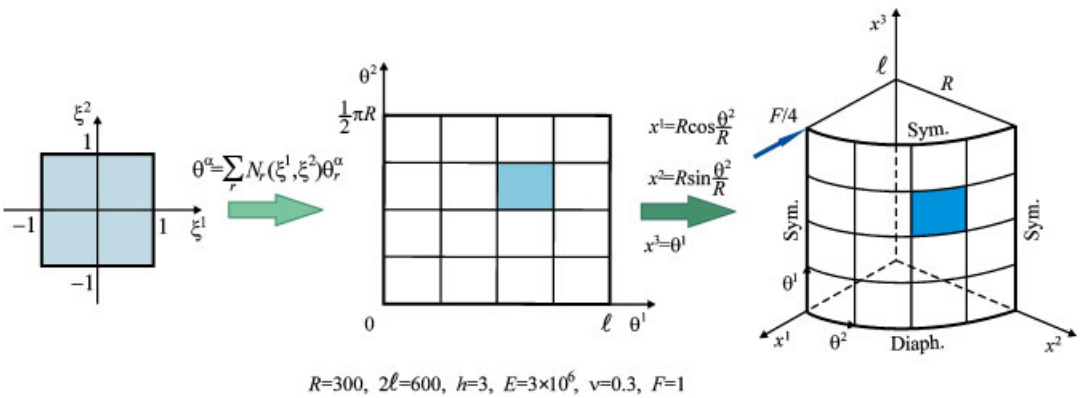

Figure 10. Pinched cylindrical shell with rigid diaphragms.

Table VII. Normalized transverse displacement at the load point of the pinched cylindrical shell.

	EXG shell elements				Isoparametric shell elements			
Mesh	EXG4A	EXG4Aσ	EXG4Aε	EXG4A$\sigma\varepsilon$	ISO4SRI	ISO4URI	ISO4A	ISO4Aσ
4×4	0.8549	0.8978	0.8875	0.8875	0.373	0.469	0.370	0.399
8×8	0.9225	0.9431	0.9390	0.9390	0.747	0.791	0.740	0.763
16×16	0.9772	0.9852	0.9836	0.9836	0.935	0.946	0.930	0.935

we consider one of the most demanding standard tests. A short cylindrical shell supported by two rigid diaphragms at the ends is loaded by two opposite concentrated loads in its middle section as depicted in Figure 10. The non-vanishing geometrical parameters of the shell can be written as follows:

$$\Gamma^3_{22}=-\frac{1}{R},\quad b^2_2=-\frac{1}{R},\quad \sqrt{a}=1,\quad m^1_1=m^2_2=1. \tag{85}$$

Owing to symmetry of the problem, only one octant of the shell is modeled with regular meshes of developed elements. Table VII lists the normalized transverse displacement under the applied load and a comparison with the above isoparametric four-node shell elements. The displacements are normalized with respect to the analytical solution -1.8248×10^{-5} [34] based on the Kirchhoff–Love shell theory. It is seen that our results exhibit an excellent agreement even for coarse meshes.

We study next the sensitivity of the EXG4Aσ element with respect to distortion parameters d_n and Δ_n depending on a single distortion parameter Δ as shown in Figure 11, which varies in a range of $0\leqslant\Delta\leqslant0.5$. For this purpose the distorted $4n\times4n$ element meshes in the parent domain in (θ^1,θ^2)-space similar to those used in Figure 8 are employed. Figure 12 displays results of the convergence study due to mesh refinement and mesh distortion considering the transverse displacement and the normal force $N_{\alpha\alpha}=H^-_{\alpha\alpha}+H^+_{\alpha\alpha}$. For computing stress resultants $H^-_{\alpha\alpha}$ and $H^+_{\alpha\alpha}$, the assumed stress distributions throughout the element (63) are utilized. One can observe that the results in Figure 12(a) corresponding to the sufficiently large distortion parameter of 0.3 are better

DOI: 10.1002/nme

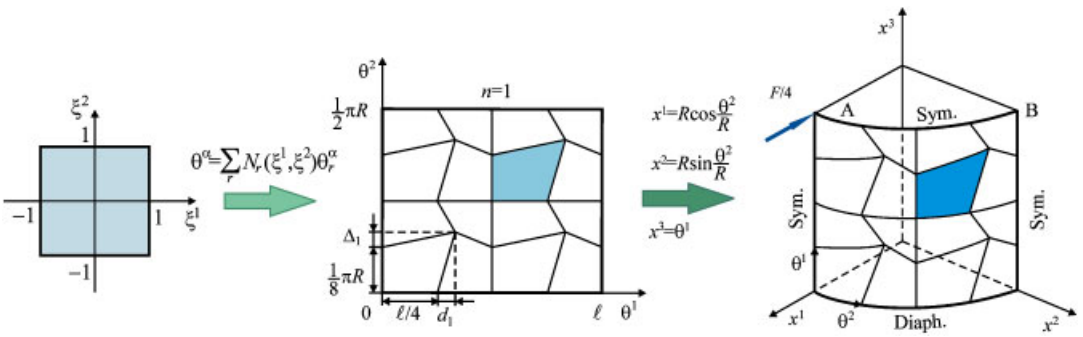

Figure 11. Pinched cylindrical shell with distorted $4n\times 4n$ meshes, where the distortion parameters $d_n=\ell\Delta/4n$ and $\Delta_n=\pi R\Delta/8n$ $(n=1,2,\ldots,10;\ \Delta\in[0,0.5])$.

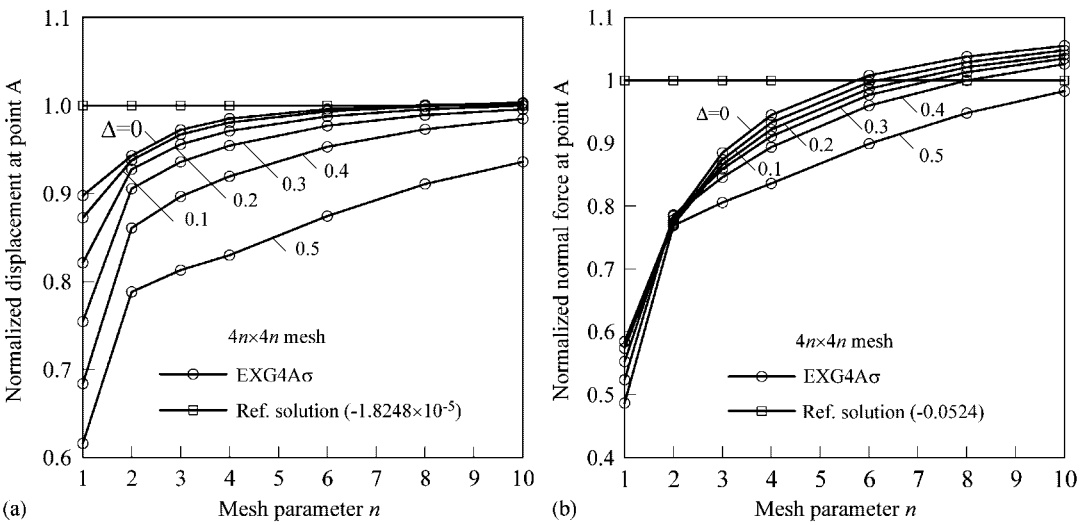

Figure 12. Convergence study due to mesh refinement and mesh distortion for a pinched cylindrical shell: (a) transverse displacement and (b) meridional force N_{11}, where the reference solution is provided by Lindberg *et al.* [34].

than those derived in [19, 29–31] by using undistorted meshes with $\Delta=0$. It is also seen in Figure 12(b) that the solution found by the EXG4Aσ element exceeds the analytical one for the normal force; a similar result has been reported in [35]. This is due to the shell theory employed in [34] for the analytical developments, which does not account for transverse shear strains. Figure 13 presents the distribution of the transverse displacement and both normal forces at the middle span AB, i.e. along the circumferential coordinate θ^2 depending on mesh configurations used. As can be seen, the EXG4Aσ element predicts the behavior of stress resultants of the pinched cylindrical shell well. The analytical solution is provided again by results [34].

Finally, we investigate the sensitivity of the EXG4Aσ element with respect to mesh distortion and slenderness ratio h/R. Figure 14 presents the normalized displacement at the load point derived

DOI: 10.1002/nme

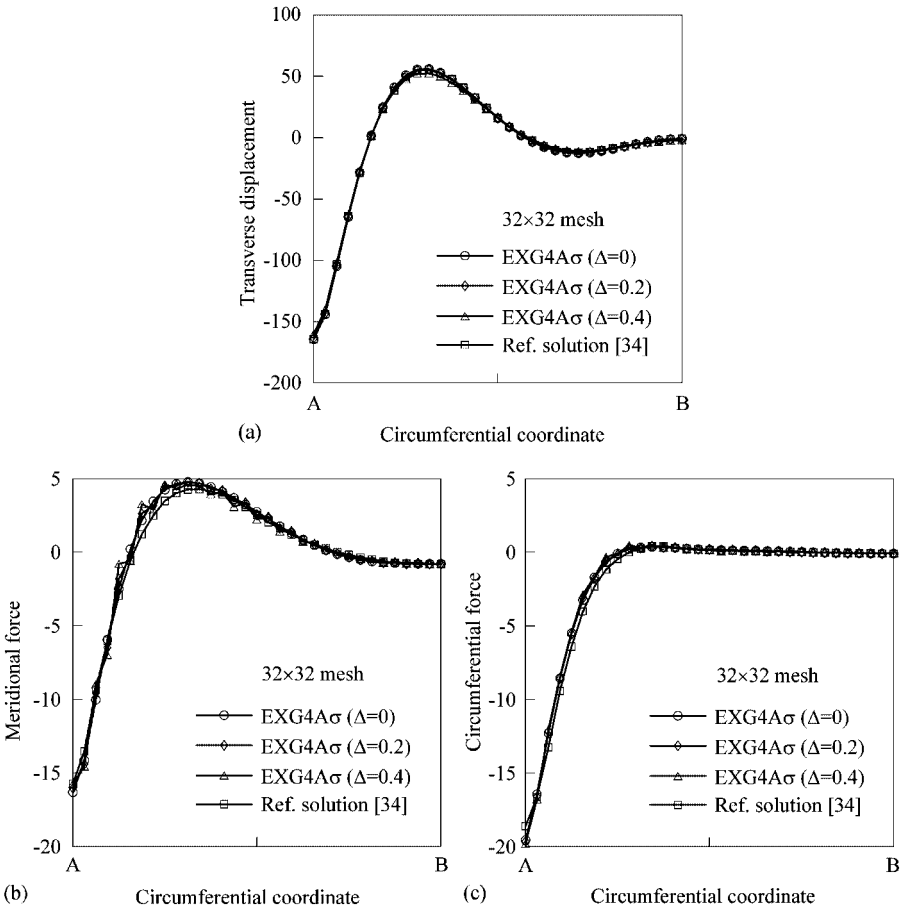

Figure 13. Results for a pinched cylindrical shell for various values of the distortion parameter: (a) transverse displacement Ehw/F, (b) meridional force RN_{11}/F and (c) circumferential force RN_{22}/F.

using uniform and distorted 32×32 meshes (Figure 11), whereas the slenderness ratio varies in a range of $10^{-3} \leqslant h/R \leqslant 10^{-1}$. As expected, the developed element is too stiff when large values of the distortion parameter Δ and small values of the slenderness ratio are employed simultaneously. The better results one can achieve if more accurate element meshes are used.

7.4. Spiral cylindrical shell

Consider a spiral surface cut out the cylindrical surface such that it is bounded by two pairs of opposite circular arcs and spiral arcs as depicted in Figure 15. The first pair of arcs is assumed to be clamped, whereas the second pair remains free. A shell is subjected to uniformly distributed transverse loading p. This problem is particularly challenging for the EXG shell element because applying the parameterization I typical of the cylindrical surface (85) leads to the necessity of using the parallelogram as a parent domain in (θ^1, θ^2)-space. However, one can deal with the

DOI: 10.1002/nme

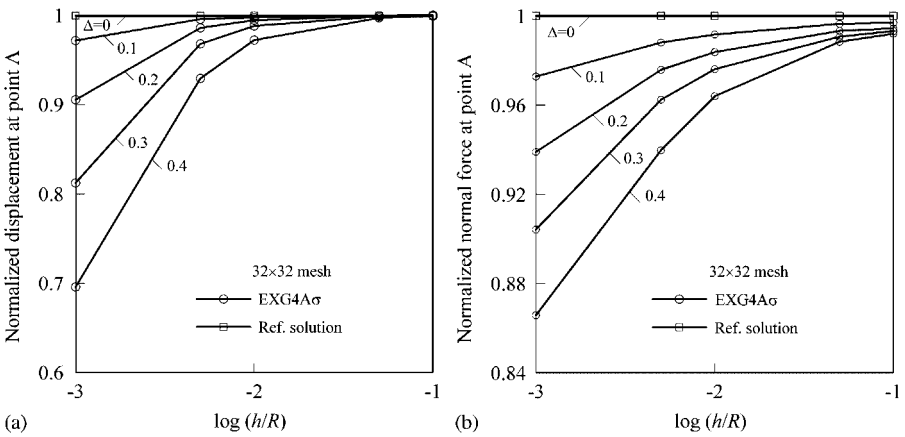

Figure 14. Results for a pinched cylindrical shell for various values of the slenderness ratio and the distortion parameter: (a) normalized transverse displacement and (b) normalized circumferential force N_{22}.

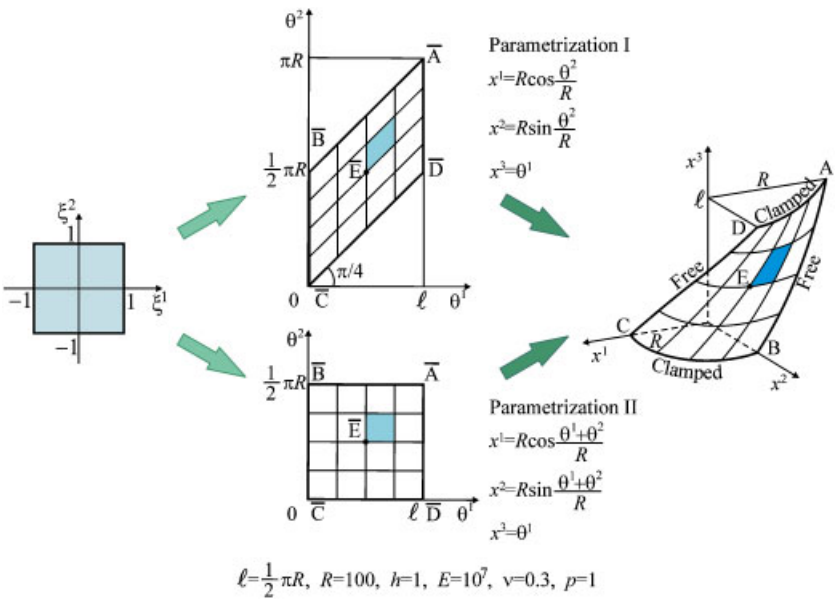

Figure 15. Spiral cylindrical shell.

square as a parent domain considering a slightly more complex parameterization II described in Figure 15. The non-vanishing geometrical parameters of the shell in such case will be

$$\Gamma^3_{11}=\Gamma^3_{22}=\Gamma^3_{12}=-\frac{1}{R},\quad b^2_1=b^2_2=-\frac{1}{R},\quad \sqrt{a}=1,\quad m^1_1=m^2_2=1,\quad m^2_1=-1. \tag{86}$$

DOI: 10.1002/nme

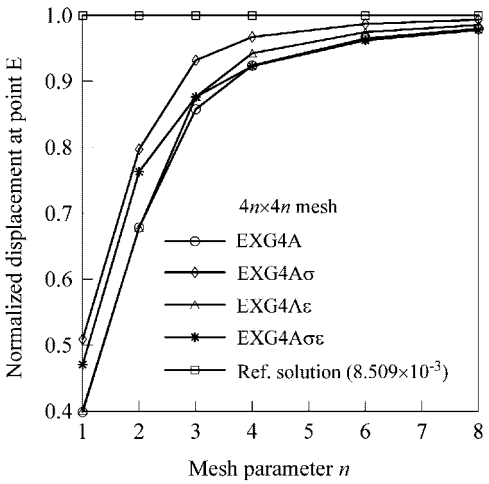

Figure 16. Convergence study due to mesh refinement for a spiral cylindrical shell, where the reference solution is provided by the 64×64 mesh of EXG4Aσ elements.

Figure 16 presents results of the convergence study for both surface parameterizations by means of the transverse displacement at a center point E. It is apparent that a transverse direction at this point coincides with x^2-direction exactly. For both parameterizations utilized the reference displacement values $w_{\mathrm{I}}(E)=8.5090527880\times10^{-3}$ and $w_{\mathrm{II}}(E)=8.5090527882\times10^{-3}$ have been found by 64×64 meshes of EXG4Aσ elements. These results demonstrate convincingly to the reader that the EXG shell element formulation developed has high potential for handling practical engineering problems.

8. CONCLUSIONS

This paper presents a newly developed family of ANS four-node EXG shell elements based on the 5-parameter shell formulation in general convected curvilinear coordinates. A family consists of four ANS elements, namely, pure displacement-based element and hybrid stress, hybrid strain and hybrid stress–strain ones. All EXG shell elements exhibit an excellent performance in the case of distorted coarse mesh configurations. But the best performer is still the hybrid stress ANS element EXG4Aσ. This element has shown the superior performance in most benchmark examples. However, the evaluation of its stiffness matrix requires the numerical matrix inversion. The hybrid stress–strain ANS element EXG4A$\sigma\varepsilon$ demonstrates a slightly less performance but does not require the expensive numerical matrix inversion. We appreciate this property very much and recommend the EXG4A$\sigma\varepsilon$ element for engineering implementations.

ACKNOWLEDGEMENTS

The support of this research by Russian Foundation for Basic Research (RFBR) under Grant No 08-01-00373 and by Russian Ministry of Education and Science under Grant No. 2.1.1/660 is gratefully acknowledged.

DOI: 10.1002/nme

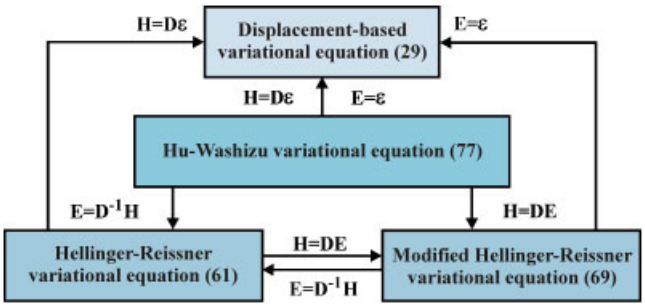

Figure A1. Interconnection of utilized variational equations.

APPENDIX A

Herein, we describe the interconnection between the displacement-based and mixed variational equations employed in Sections 5 and 6 for developments of the EXG shell element formulations. They are displayed in Figure A1.

REFERENCES

1. Ahmad S, Irons BM, Zienkiewicz OC. Analysis of thick and thin shell structures by curved finite elements. *International Journal for Numerical Methods in Engineering* 1970; **2**:419–451.
2. Bathe KJ. *Finite Element Procedures*. Prentice-Hall: Englewood Cliffs, NJ, 1996.
3. Belytschko T, Liu WK, Moran B. *Nonlinear Finite Elements for Continua and Structures*. Wiley: New York, 2000.
4. Hughes TJR. *The Finite Element Method*: *Linear Static and Dynamic Finite Element Analysis*. Prentice-Hall: Englewood Cliffs, NJ, 1987.
5. Zienkiewicz OC, Taylor RL. *The Finite Element Method. Volume 1*: *The Basis* (5th edn). Butterworth Heinemann: Oxford, 2000.
6. Kulikov GM, Plotnikova SV. Efficient mixed Timoshenko–Mindlin shell elements. *International Journal for Numerical Methods in Engineering* 2002; **55**:1167–1183.
7. Kulikov GM, Plotnikova SV. Simple and effective elements based upon Timoshenko–Mindlin shell theory. *Computer Methods in Applied Mechanics and Engineering* 2002; **191**:1173–1187.
8. Cho M, Roh HY. Development of geometrically exact new shell elements based on general curvilinear coordinates. *International Journal for Numerical Methods in Engineering* 2003; **56**:81–115.
9. Kulikov GM, Plotnikova SV. Non-linear strain-displacement equations exactly representing large rigid-body motions. Part I: Timoshenko–Mindlin shell theory. *Computer Methods in Applied Mechanics and Engineering* 2003; **192**:851–875. Part II: enhanced finite element technique 2006; **195**:2209–2230; Part III: analysis of TM shells with constraints 2007; **196**:1203–1215.
10. Roh HY, Cho M. The application of geometrically exact shell elements to B-spline surfaces. *Computer Methods in Applied Mechanics and Engineering* 2004; **193**:2261–2299.
11. Kulikov GM, Plotnikova SV. Finite rotation geometrically exact four-node solid-shell element with seven displacement degrees of freedom. *Computer Modeling in Engineering and Sciences* 2008; **28**:15–38.
12. Kulikov GM, Carrera E. Finite deformation higher-order shell models and rigid-body motions. *International Journal of Solids and Structures* 2008; **45**:3153–3172.
13. Buechter N, Ramm E. Shell theory versus degeneration—a comparison in large rotation finite element analysis. *International Journal for Numerical Methods in Engineering* 1992; **34**:39–59.
14. Kulikov GM, Plotnikova SV. Non-linear geometrically exact assumed stress–strain four-node solid-shell element with high coarse-mesh accuracy. *Finite Elements in Analysis and Design* 2007; **43**:425–443.
15. Grigolyuk EI, Kulikov GM, Plotnikova SV. Contact problem for a pneumatic tire interacting with a rigid foundation. *Mechanics of Composite Materials* 2004; **40**:427–436.

DOI: 10.1002/nme

16. Hughes TJR, Tezduyar TE. Finite elements based upon Mindlin plate theory with particular reference to the four-node bilinear isoparametric element. *Journal of Applied Mechanics* (ASME) 1981; **48**:587–596.
17. MacNeal RH. Derivation of element stiffness matrices by assumed strain distributions. *Nuclear Engineering and Design* 1982; **70**:3–12.
18. Bathe KJ, Dvorkin EN. A four-node plate bending element based on Mindlin/Reissner plate theory and a mixed interpolation. *International Journal for Numerical Methods in Engineering* 1985; **21**:367–383.
19. Bathe KJ, Dvorkin EN. A formulation of general shell elements—the use of mixed interpolation of tensorial components. *International Journal for Numerical Methods in Engineering* 1986; **22**:697–722.
20. MacNeal RH, Harder RL. A proposed standard set of problems to test finite element accuracy. *Finite Elements in Analysis and Design* 1985; **1**:3–20.
21. Pian THH. Derivation of element stiffness matrices by assumed stress distributions. *AIAA Journal* 1964; **2**:1333–1336.
22. Pian THH, Sumihara K. Rational approach for assumed stress finite elements. *International Journal for Numerical Methods in Engineering* 1984; **20**:1685–1695.
23. Pian THH. State-of-the-art development of hybrid/mixed finite element method. *Finite Elements in Analysis and Design* 1995; **21**:5–20.
24. Lee SW, Pian THH. Improvement of plate and shell finite elements by mixed formulations. *AIAA Journal* 1978; **16**:29–34.
25. Rhiu JJ, Lee SW. A new efficient mixed formulation for thin shell finite element models. *International Journal for Numerical Methods in Engineering* 1987; **24**:581–604.
26. Wempner G, Talaslidis D, Hwang CM. A simple and efficient approximation of shells via finite quadrilateral elements. *Journal of Applied Mechanics* (ASME) 1982; **49**:115–120.
27. Chapelle D, Bathe KJ. *The Finite Element Analysis of Shells—Fundamentals*. Springer: Berlin, 2003.
28. Washizu K. *Variational Methods in Elasticity and Plasticity* (3rd edn). Pergamon Press: Oxford, 1982.
29. Simo JC, Fox DD, Rifai MC. On a stress resultant geometrically exact shell model. Part II: the linear theory; computational aspects. *Computer Methods in Applied Mechanics and Engineering* 1989; **73**:53–92.
30. Hughes TJR, Liu WK. Nonlinear finite element analysis of shells. Part II: two-dimensional shells. *Computer Methods in Applied Mechanics and Engineering* 1981; **27**:167–181.
31. Liu WK, Law ES, Lam D, Belytschko T. Resultant-stress degenerated-shell element. *Computer Methods in Applied Mechanics and Engineering* 1986; **55**:259–300.
32. Timoshenko SP, Woinowsky-Krieger S. *Theory of Plates and Shells* (2nd edn). McGraw-Hill: New York, 1970.
33. Belytschko T, Wong BL, Stolarski H. Assumed strain stabilization procedure for the 9-node Lagrange shell element. *International Journal for Numerical Methods in Engineering* 1989; **28**:385–414.
34. Lindberg GM, Olson MD, Cowper GR. New developments in the finite element analysis of shells. *Quarterly Bulletin of Division of Mechanical Engineering and National Aeronautical Establishment*, *National Research Council of Canada* 1969; **4**:1–38.
35. Briassoulis D. The four-node C^0 shell element reformulated. *International Journal for Numerical Methods in Engineering* 1996; **39**:2417–2455.

DOI: 10.1002/nme